Papers in the Earth and Atmospheric Sciences

Earth and Atmospheric Sciences, Department of

2-2010

Coupled carbon isotopic and sedimentological records from the Permian system of eastern Australia reveal the response of atmospheric carbon dioxide to glacial growth and decay during the late Paleozoic Ice Age

Lauren P. Birgenheier
University of Nebraska-Lincoln, Lauren.Birgenheier@utah.edu

Tracy D. Frank
University of Nebraska-Lincoln, tfrank2@unl.edu

Christopher R. Fielding
University of Nebraska-Lincoln, cfielding2@unl.edu

Michael C. Rygel
State University of New York at Potsdam, rygelmc@potsdam.edu

Coupled carbon isotopic and sedimentological records from the Permian system of eastern Australia reveal the response of atmospheric carbon dioxide to glacial growth and decay during the late Paleozoic Ice Age

Lauren P. Birgenheier,[1] Tracy D. Frank,[1] Christopher R. Fielding,[1] and Michael C. Rygel [2]

1. Department of Geosciences, University of Nebraska–Lincoln, Lincoln, NE 68588, USA
2. Department of Geology, State University of New York at Potsdam, 44 Pierrepont Avenue, Potsdam, NY 13676, USA

Corresponding author — L. P. Birgenheier. Present address: Energy & Geoscience Institute, University of Utah,
423 Wakara Way, Suite 300, Salt Lake City, UT 84108, USA; LBirgenheier@egi.utah.edu

Abstract
Proxy geochemical records from high-latitude, ice-proximal deposits have the potential to provide key insights into past icehouse climates, but such records are rare. The Permian System of eastern Australia contains a rich record of environmental and climatic changes that occurred in areas proximal to glaciation during the acme and waning stages of the late Paleozoic ice age. Within this succession, a wealth of fine-grained, organic matter-rich facies provides an opportunity to construct a bulk $\delta^{13}C_{org}$ record that records changes in atmospheric CO_2 through the Permian. Fluctuations in $\delta^{13}C_{org}$ track changes in climate determined independently on the basis of sedimentological criteria in the same strata. These patterns are also broadly consistent with multiple proxy records derived from paleoequatorial sites. The results of this geochemical investigation 1) support recent studies using the high-latitude, ice-proximal, sedimentologic and stratigraphic record and paleoequatorial geochemical proxies that document highly variable climatic conditions within the overall Permian icehouse-to-greenhouse transition, and 2) confirms that the sedimentary record of glaciation from eastern Australia reflects global changes in atmospheric CO_2 on several m.y.-order timescales.

Keywords: Permian, Late Paleozoic, carbon isotope, organic matter, climate, Gondwana

1. Introduction

Few complete late Paleozoic, high-latitude, stable isotopic records have been derived or constructed from stratigraphic successions that formed in areas proximal to glaciation (Scheffler et al., 2003; Korte et al., 2008). Moreover, none of these stable isotopic records are linked directly to the sedimentology of the successions from which they were sampled. Rather, current understanding of past icehouse climates, in particular the late Paleozoic ice age, relies primarily on proxy records derived from paleoequatorial deposits (Grossman et al., 1993; Veizer et al., 1999; Mii et al., 1999, 2001; Bruckschen et al., 1999; Saltzman, 2002, 2003; Korte et al., 2005). Difficulties in correlating between the low and high latitudes, however can result in contradictory interpretations (Figure 1).

Although a robust, high latitude sedimentary record of the late Paleozoic ice age exists in eastern Australia (Fielding et al., 2008a, 2008b), the relative scarcity of carbonate in these strata (Rogala et al., 2007; James et al., 2009) has made it difficult to construct isotopic records that are representative of the interval as a whole (Korte et al., 2008). However, this same succession contains numerous organic-matter-rich intervals that allow construction of a new bulk organic carbon isotope curve.

Previous work by Fielding et al. (2008a, 2008b) provides a robust framework for interpretation of the results. The sedimentologic and stratigraphic record of glaciation from eastern Australia is the most highly resolved regional record of the late Paleozoic ice age available to date. In eastern Australia, the Permian System records four temporally discrete glacial intervals that spanned Asselian through Capitanian time (Fielding et al., 2008a, 2008b). Within this mainly marine succession, evidence for glacial activity is recorded by the presence of diamictites, outsized clasts in fine-grained, offshore facies (interpreted as ice-rafted debris), pseudomorphs after the cold-water mineral ikaite (Shearman and Smith, 1985), iceberg keel structures, and evidence for abrupt, large-scale shifts in base level (Fielding et al., 2006, 2008a, 2008b; Birgenheier, 2007; Rygel et al., 2008; Birgenheier et al., 2009). Intervening non-glacial intervals are recorded by fluvial to shallow marine facies with no evidence of glacial influence (Fielding et al., 2008a, 2008b). Using the regional time-space distribution of glacial and non-glacial facies constrained by radiogenic isotopic and biostratigraphic data, the timing and duration of glacial intervals have been determined as follows: P1, Asselian–early Sakmarian; P2, latest Sakmarian–early Artinskian; P3, late Kungurian–Roadian; and P4, mid Wordian–Capitanian (Figure 2a) (Fielding et al., 2008a, see supplemental materials for detailed documentation;
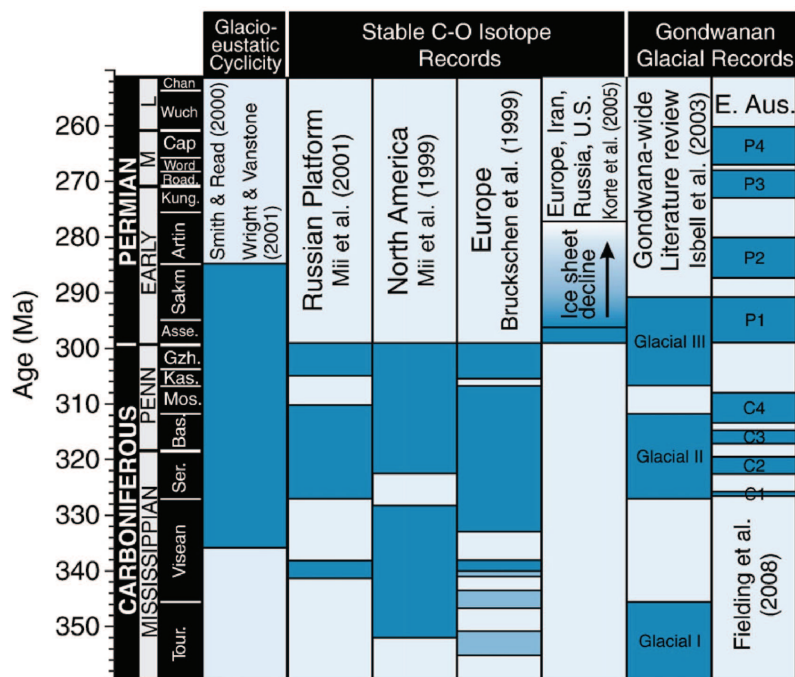
Figure 1. Estimates of the duration of the late Paleozoic ice age (LPIA), or glacial episodes within the LPIA (shaded intervals), as determined from: 1) indirect records of glaciation, such as paleoequatorial cyclothemic and stable isotopic records, and 2) direct ice-proximal sedimentary records of glaciation. Note the discrepancy between those estimates based on paleoequatorial stable isotope records, highlighting the need for a stable isotope record that can be directly tied to the high-latitude record of glaciation, as presented in this study.

Fielding et al., 2008b). Glacial intervals were ~ 5–7 m.y. in duration, with alternating non-glacial intervals of similar duration. Importantly, these periods were not glacial-interglacial cycles in the sense of the Pleistocene, but much longer on 10^6-yr.-order timescales (Fielding et al., 2008a, 2008b; Birgenheier et al., 2009). Glacial intervals P1 and P2 were the most intense, with evidence for the development of widespread ice sheets, whereas epochs P3 and P4 were likely confined to alpine-style glaciation (Fielding et al., 2008a, 2008b). Younger, post-Capitanian strata record climate amelioration and a shift toward a protracted greenhouse climate state, as indicated by numerous records across Gondwana (Montañez et al., 2007). Thus, the Permian succession of eastern Australia provides a record of dynamic and fluctuating climate conditions, specifically glacial and non-glacial conditions that alternated during a longer-term global transition from icehouse to greenhouse conditions. We seek to examine how changes in the $\delta^{13}C_{org}$ record compare to climatic changes interpreted from the sedimentologic and stratigraphic record from same region.

2. Regional geologic setting

The Bowen–Gunnedah–Sydney Basin System (BGSBS) spanned polar to temperate latitudes during the Permian and preserves strata that were deposited on an open marine shelf that faced the Panthalassan Ocean. The BGSBS can be divided into three main phases of geologic development: 1) extension during the late Carboniferous to early Permian with deposition in a series of discontinuous basins that became connected over time with successive marine transgressions, 2) short-lived passive, thermal subsidence during the mid-Permian in which offshore marine deposition dominated, and 3) foreland crustal loading (induced by the Hunter–Bowen Orogeny), which resulted in marine basin infilling during the late Permian to Middle Triassic (Fielding et al., 2001).

Permian units of the Sydney and Bowen Basins define an eastward or seaward thickening clastic wedge. In general, eastern Australia was dominated by siliciclastic deposition during the Permian with areally-restricted carbonate deposition on paleotopographic highs and/or areas sheltered from the abundant

terrigenous input that characterized much of the basin (Fielding et al., 2001; James et al., 2009).

The ten studied Permian units in the BGSBS, listed in Table 1, collectively contain both glacial and non-glacial facies, as identified by Fielding et al. (2008a, 2008b) (Figure 2a). The age of the formations range from mid-Sakmarian to lowermost Wuchiapingian, spanning glacial intervals P2–P4 and intervening non-glacial intervals (*sensu* Fielding et al., 2008a, 2008b), with near-complete coverage of the time period except for a ~ 3.5 m.y. gap that extends from the Roadian to early Wordian (Figure 2).

3. Methods

Samples (25–50 cm^3) of organic-rich facies were collected from ten Permian formations. Lithologies collected include grey siltstone, interlaminated sandstone and siltstone, and diamictite. Samples were collected from a combination of core and outcrop localities in three regions throughout Queensland and New South Wales, with the majority of sampling restricted to the southeastern Sydney Basin (Table 1; Figure 2). Construction of measured sections accompanied sampling so that samples could be tied directly back to their sedimentologic and stratigraphic context.

In preparation for analysis of total organic carbon (C_{org}), total nitrogen (N_{tot}), and $\delta^{13}C$ and $\delta^{14}N$ values of bulk organic matter, samples were rinsed with deionized water to remove any surface salts, dried at 50 °C, and powdered. Between 10 and 44 mg of each sample was weighed into a 5 × 9 mm^2 silver-foil cup. The inorganic carbon fraction of each sample was removed using the vapor acidification method of Hedges and Stern (1984).

Within 24–48 hours of acidification, at total of 175 samples were analyzed using a Costech Instruments Element Analyzer connected to a Thermo Finnigan MAT 253 stable-isotope gas-ratio mass spectrometer at the University of Kansas stable isotope laboratory. C_{org}, N_{tot}, and $\delta^{13}C_{org}$ values were calculated using the measured total original sample mass before vapor acidification treatment. Analytical precision (1σ) for determinations of C_{org} and N_{tot} contents are 2.66 and 4.30 wt.%, respectively. The precision (1σ) of calculated C_{org}/N_{tot} ratios is
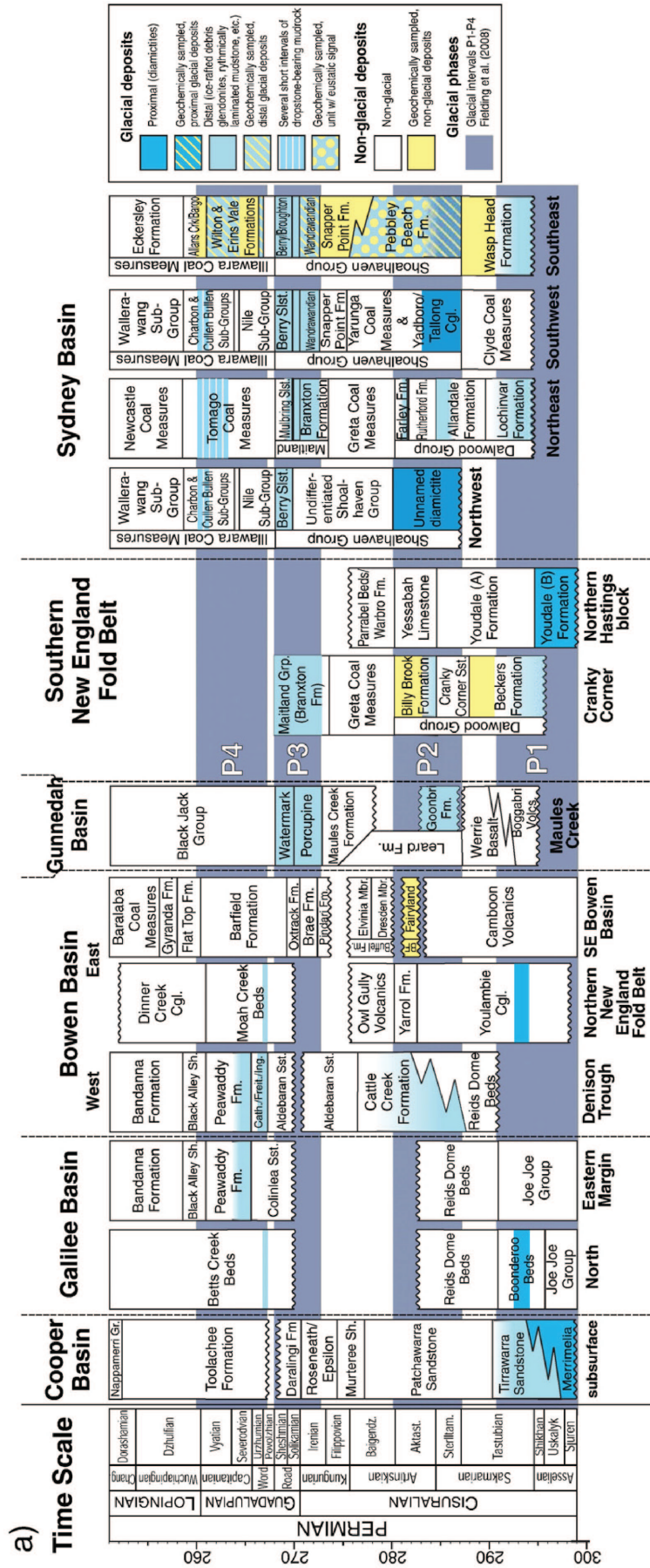
Figure 2. a) Permian stratigraphic record of glaciation from eastern Australia (Fielding et al., 2008a, 2008b). Constructed from documented biostratigraphic and geochronologic age constraints. See Fielding et al. (2008a, supplemental paper) for details. Permian timescale for this manuscript follows Gradstein et al. (2004). Units sampled for this study are highlighted with some element of black. Both "glacial" and "non-glacial" units (*sensu* Fielding et al., 2008a, 2008b) were sampled. **b)** Sampling regions for this study highlighted in dark grey. See Table 1 for more specific locality information. Grey shaded regions represent all the regions in eastern Australia that were examined in the construction of the stratigraphic record of glaciation (Figure 2a), as published by Fielding et al. (2008a).

Figure 2. (continued)
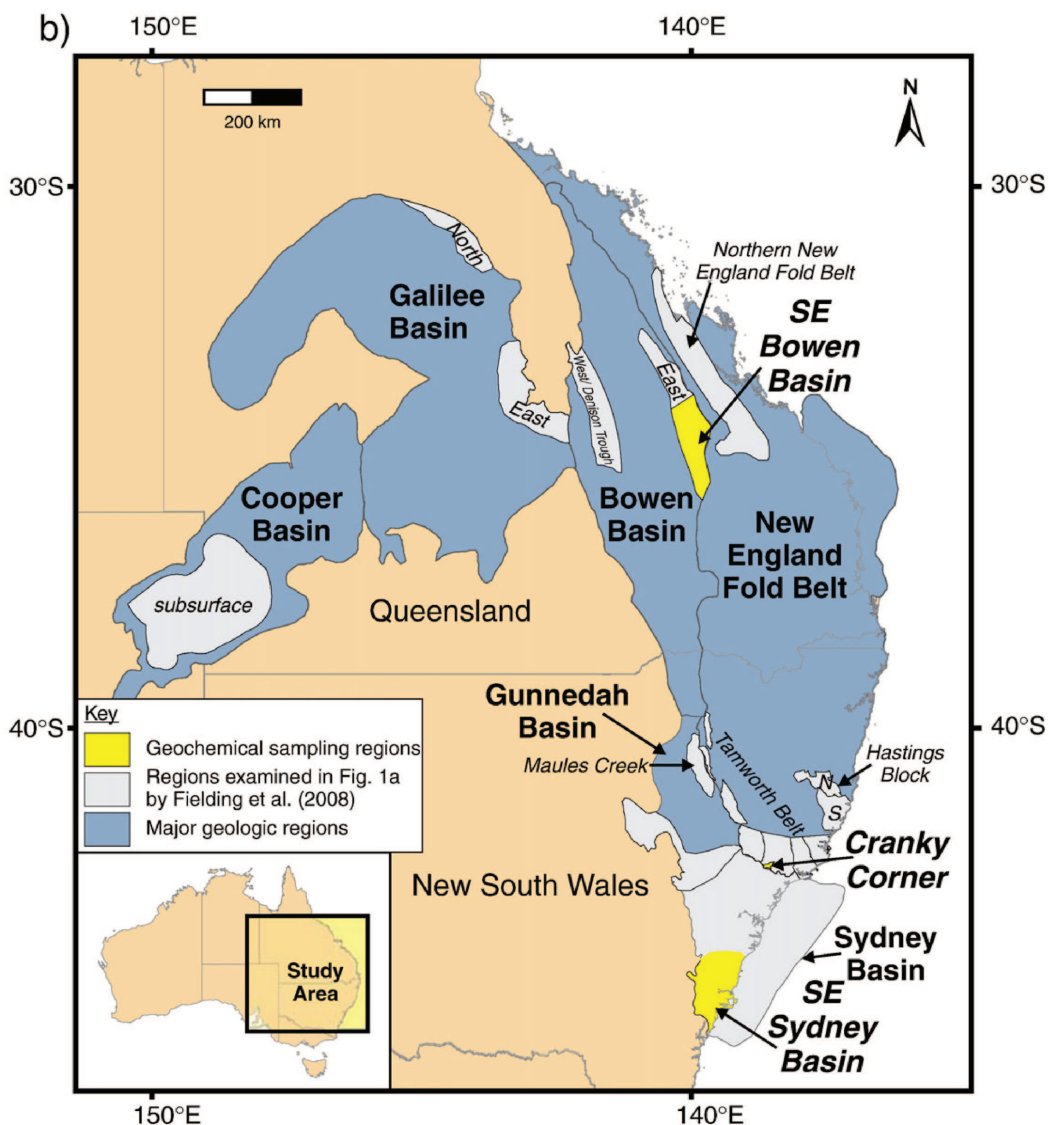
Table 1. Geochemical sampling localities in eastern Australia: organic matter-rich facies collected.

Formation	Group	Region	Outcrop/core locality
Fairyland mbr. of Buffel Fmn.		SE Bowen Basin, QLD	Mundubbera-11 core, south of Cracow at Cracow Homestead Lat./long.: 25° 22′ S, 150° 17′ E
Beckers Fmn.	Dalwood Grp.	Cranky Corner, NSW	DM Tangorin DDH1 core 55 km NW of Newcastle, 10 km N of Branxton
Billy Brook Fmn.	Dalwood Grp.	Cranky Corner, NSW	DM Tangorin DDH1 core 55 km NW of Newcastle, 10 km N of Branxton
Wasp Head Fmn.		SE Sydney Basin, NSW	South Pebbles Beach, GPS: 56H 573, 553 Emily Miller Beach, GPS: 56H 556, 486
Pebbley Beach Fmn.	Shoalhaven Grp.	SE Sydney Basin, NSW	South Pebbles to North Depot Beach, GPS: 56H 573, 553 to 56H 576, 538 Mill Point to Clear Point, GPS: 56H 582, 562 to 592, 568
Snapper Point Fmn.	Shoalhaven Grp.	SE Sydney Basin, NSW	Snapper Point, GPS: 56H 617, 606 Pretty Beach, GPS: 56H 612, 603 Bannister's Point, GPS: 56H 713, 877
Wandrawandian Sltstn.	Shoalhaven Grp.	SE Sydney Basin, NSW	Elecom Clyde River-11 core, near Tomerong village GPS: 56H 798, 182
Erins Vale Fmn.	Illawara Coal Measures	SE Sydney Basin, NSW	Pacific Power Hawkesbury - Bunnerong DDH1 Matraville, NSW, 13 km SSE of Sydney city center
Wilton Fmn.	Illawara Coal Measures	SE Sydney Basin, NSW	Pacific Power Hawkesbury - Bunnerong DDH1 Matraville, NSW, 13 km SSE of Sydney city center
Bargo Claystone	Illawara Coal Measures	SE Sydney Basin, NSW	Pacific Power Hawkesbury - Bunnerong DDH1 Matraville, NSW, 13 km SSE of Sydney city center

NSW = New South Wales; QLD = Queensland.

5.06% when the errors of C_{org} and N_{tot} measurements are propagated. Carbon isotopic compositions of the bulk organic matter fractions are reported in per mil (‰) relative to the Vienna Peedee Belemnite standard (V-PDB). Analytical precision, based on the repeated measurement of an internal standard, acetanellide ($\delta^{13}C_{acetanellide}$ = −29.8‰), for $\delta^{13}C_{org}$ values is ± 0.3‰ (*n* = 15). Replicate analyses were performed for every 10 samples that were run. Reproducibility of duplicate samples, the average difference between duplicate and original samples, is 0.03% ± 0.04% (1σ) and 0.04‰ ± 0.03‰ (1σ) for %C_{org} and $\delta^{13}C_{org}$, respectively. The difference between %N_{tot} of the duplicates and the original sample was negligible (0.0007% ± 0.0006%).

4. Results

The C_{org} contents range from 0.2 to 15.9 wt.%, with an average of 2.0% ± 1.8% (1σ). N_{tot} contents range from 0.01 to 0.43 wt.%, averaging 0.10 ± 0.06% (1σ). The C_{org}/N_{tot} ratios range from 2.6 to 39.6 wt.% (average 19.9 ± 7.0%: 1σ). The $\delta^{13}C_{org}$ values range from −27.9‰ to −21.6‰. The average value for the data set is −23.7 ± 1.1‰ (1σ). The full dataset can be viewed in Table 2.

Results are plotted in Figure 3. The %C_{org} and %N_{tot} data exhibit a significant linear covariance (r^2 = 0.81), with higher C_{org} values corresponding to higher N_{org} (Figure 3b). A weaker positive relationship exists between C_{org}/N_{tot} and %C_{org} (r^2 = 0.56) (Figure 3c). There are no statistically significant linear relationships between $\delta^{13}C_{org}$ and C_{org}/N_{tot} (r^2 = 0.04) (Figure 3a) or $\delta^{13}C_{org}$ and %C_{org} (r^2 = 0.30) (Figure 3d).

Temporal variations in the measured parameters were determined by plotting data versus stratigraphic height converted to age (Figure 4). Age was calculated by assuming a linear sedimentation rate between tie points of known age (i.e., formation boundaries) based on available biostratigraphic and geochronological data (Figure 2a). A 1 m.y. running average trendline was plotted to highlight temporal trends (Figure 4).

Mid- to upper Sakmarian strata, including the Beckers Formation (Cranky Corner) and the Wasp Head and the lower Pebbley Beach Formations (Sydney Basin), are characterized by C_{org}/N_{tot} ratios generally ≤ 25 (Figure 4). Artinskian–lowermost Kungurian strata have somewhat higher C_{org}/N_{tot} ratios, generally ≥ 20 (Figure 4). This time interval is represented by the middle-upper Pebbley Beach Formation and the lower half of the Snapper Point Formation (Sydney Basin), the Billy Brook Formation (Cranky Corner), and the Fairyland Member (Bowen Basin). Upper Kungurian strata, the upper Snapper Point Formation and the Wandrawandian Siltstone (Sydney Basin), are characterized by C_{org}/N_{tot} ratios that generally lie between 10 and 20 (Figure 4). Mid-Wordian to basal Wuchiapingian strata of the Illawarra Coal Measures (Erins Vale Formation, Wilton Formation and Bargo Claystone) display C_{org}/N_{tot} ratios ≤ 20, with some samples ≤ 10 (Figure 4).

Positive excursions in $\delta^{13}C_{org}$ values occur in mid- to upper Sakmarian (shift A: magnitude 3.2‰), mid-Kungurian (shift C: magnitude 2.3‰), and upper Wordian (shift E: magnitude 1‰) strata (Figure 4). Positive shifts A, C, and E, occur at the onset of glacial intervals P2, P3, and P4 of Fielding et al. (2008a, 2008b, and 2008c, respectively) (Figure 4). Negative shifts characterize upper Artinskian (B: magnitude 4.3‰), upper Kungurian (D: magnitude 3.7%), and the lower Capitanian (F: magnitude 1.5‰) strata (Figure 4). Negative shifts B, D, and F, occur during the middle to end of glacial intervals P2, P3, and P4, respectively (Figure 4). Hence, changes in $\delta^{13}C_{org}$ exhibit a concordant relationship with documented glacial intervals P2–P4 (Figure 4). The magnitude of $\delta^{13}C_{org}$ shifts associated with each glacial interval decreases from P2 to P4 (Figure 4). Other significant isotopic shifts include a positive shift during the mid-Artinskian (at the end of the P2 glacial

interval), and a late Artinskian negative excursion followed by a return to more positive values (during the non-glacial interval between P2 and P3) (Figure 4).

5. Interpretation

The isotopic composition of marine and terrestrial bulk organic matter is controlled by a number of variables: organic matter source, local or regional environmental effects, and fluxes between global carbon reservoirs (Meyers, 1997; Hayes et al., 1999; Gröcke, 2002). Global changes in carbon cycling may be related to climatic changes, such as changes in atmospheric pCO_2 as a result of increased organic carbon burial. Some techniques have been developed to control for organic matter source and some environmental effects in which isotopic analysis is performed on specific organic matter components (e.g. specific maceral types, fossil wood or plants, and sedimentary alkenones), so that carbon isotopic shifts can be related to global changes in carbon cycling (e.g. Gröcke et al., 1999, 2002; Pagani, 2002; Gröcke et al., 2005; Rimmer et al., 2006). As compared to isotopic analysis of bulk organic matter, these newer methods greatly reduce uncertainty and simplify interpretation of $\delta^{13}C_{org}$ curves, but their application is limited to successions that contain proper sampling materials. The Permian record from eastern Australia does contain some identifiable fossil wood and coals but they are not stratigraphically continuous, offering a discontinuous carbon isotopic record, at best. Additionally, marine organic matter within the succession is too old to host sedimentary alkenones (Pagani, 2002). However, organic-rich facies are fairly ubiquitous throughout the Permian record. Isotopic analysis of bulk organic matter, while not perfect, offers a good first approximation of secular variations in $\delta^{13}C_{org}$ (e.g. Scheffler et al., 2003), which may offer important information about climatic variation during the Permian, particularly when coupled with the sedimentary record of glacial and non-glacial deposits from the same region.

5.1. Organic matter source

Comparison of C_{org}/N_{tot} and $\delta^{13}C$ values from the studied succession against published ranges of marine algal, C3 land plant, and lacustrine algal organic matter (Meyers et al., 1995; Meyers, 1997; Gröcke, 2002) indicates that terrigenous organic matter contributes more significantly to the succession as a whole as compared to marine organic matter (Figure 3a). Typically, marine organic matter exhibits a C_{org}/N_{tot} ≤ 10 and terrestrial organic matter, ≥ 20 (Meyers, 1997). Reported $\delta^{13}C$ values of ancient C3 plants generally lie between −23 and −27‰ (average: −24‰) (Gröcke, 2002). Marine organic matter can be expected to carry a $\delta^{13}C$ value of ~ 22‰ (Meyers, 1997). Burial diagenesis may lower C_{org}/N_{tot} values (Meyers et al., 1995), which results in a higher proportion of the samples interpreted as fully terrigenous in source (Figure 3a).

Organic matter source through the Permian succession of eastern Australia displays variability, between formations, within formations, and through time (Figure 4). For instance, organic matter within the Fairyland Member of the Buffel Formation is interpreted to be fully terrestrial, as evidenced by C_{org}/N_{tot} ratios ≥ 20 in all samples (Figure 4a) and visible macerated plant debris in hand samples. The Erins Vale Formation of the Illawara Coal Measures, with C_{org}/N_{tot} ratios ≤ 10.23 (Figure 4a), contains mostly marine organic matter. When C_{org}/N_{tot} data are examined temporally, it is evident that pre-mid-Kungurian strata contain mainly terrestrial-derived organic matter whereas organic matter in younger strata is mainly of marine origin (Figure 4a).

Table 2. Results of geochemical analysis of Permian organic-rich facies from eastern Australia.

Formation	Sample name	Age (Ma): Gradstein et al. (2004)	%C_{org}◊	%N_{total}◊	C_{org}/N_{total}	$\delta^{13}C_{org}$ (‰)*	$\delta^{15}N$ (‰)†	Locality
Beckers Fmn.	DMT 326.0	290.53	0.98	0.04	22.53	−25.09	6.09	Cranky Corner: Tangorin DDH1 core
Beckers Fmn.	DMT 326.0R	290.53	1.00	0.06	22.21	−25.11	6.09	Cranky Corner: Tangorin DDH1 core
Beckers Fmn.	DMT 323.80	290.48	0.80	0.04	19.88	−25.18	5.36	Cranky Corner: Tangorin DDH1 core
Beckers Fmn.	DMT 319.60	290.38	0.91	0.04	23.48	−24.90	3.22	Cranky Corner: Tangorin DDH1 core
Beckers Fmn.	DMT 318.37	290.36	1.24	0.06	19.73	−24.61	5.28	Cranky Corner: Tangorin DDH1 core
Beckers Fmn.	DMT 314.57	290.27	1.15	0.05	22.56	−25.78	5.76	Cranky Corner: Tangorin DDH1 core
Wasp Head Fmn.	WH-6 — 2.5	290.27	0.74	0.06	13.13	−23.76	3.95	Depot Beach
Wasp Head Fmn.	WH-6 — 0.3	290.08	0.50	0.05	10.31	−24.26	4.02	Depot Beach
Beckers Fmn.	DMT 305.40	290.06	0.90	0.06	15.52	−24.68	5.80	Cranky Corner: Tangorin DDH1 core
Beckers Fmn.	DMT 303.60	290.02	0.44	0.03	12.64	−25.49	4.98	Cranky Corner: Tangorin DDH1 core
Beckers Fmn.	DMT 298.30	289.90	0.97	0.06	17.34	−25.03	4.06	Cranky Corner: Tangorin DDH1 core
Beckers Fmn.	DMT 298.30R	289.90	1.00	0.06	16.17	−24.64	5.83	Cranky Corner: Tangorin DDH1 core
Beckers Fmn.	DMT 295.30	289.83	0.89	0.05	16.03	−24.68	6.55	Cranky Corner: Tangorin DDH1 core
Beckers Fmn.	DMT 293.56	289.79	0.96	0.06	16.64	−24.87	4.38	Cranky Corner: Tangorin DDH1 core
Beckers Fmn.	DMT 292.75	289.77	0.79	0.05	15.20	−24.67	5.58	Cranky Corner: Tangorin DDH1 core
Beckers Fmn.	DMT 290.65	289.72	0.83	0.05	15.66	−24.50	4.72	Cranky Corner: Tangorin DDH1 core
Beckers Fmn.	DMT 286.0	289.62	1.17	0.07	17.09	−24.80	4.76	Cranky Corner: Tangorin DDH1 core
Beckers Fmn.	DMT 285.60	289.61	1.00	0.06	15.92	−24.35	5.40	Cranky Corner: Tangorin DDH1 core
Beckers Fmn.	DMT 278.50	289.45	0.85	0.04	20.03	−25.34	5.13	Cranky Corner: Tangorin DDH1 core
Beckers Fmn.	DMT 274.40	289.35	0.53	0.04	13.13	−25.24	5.06	Cranky Corner: Tangorin DDH1 core
Beckers Fmn.	DMT 267.50	289.19	0.62	0.05	12.58	−25.45	4.31	Cranky Corner: Tangorin DDH1 core
Beckers Fmn.	DMT 257.95	288.98	1.29	0.07	18.66	−24.34	5.30	Cranky Corner: Tangorin DDH1 core
Beckers Fmn.	DMT 247.50	288.74	0.94	0.05	20.61	−25.39	4.78	Cranky Corner: Tangorin DDH1 core
Beckers Fmn.	DMT 240.90	288.59	1.13	0.05	21.80	−25.59	5.49	Cranky Corner: Tangorin DDH1 core
Beckers Fmn.	DMT 238.50	288.53	1.07	0.05	22.48	−25.15	5.49	Cranky Corner: Tangorin DDH1 core
Beckers Fmn.	DMT 238.50R	288.53	1.09	0.05	22.90	−25.21	5.44	Cranky Corner: Tangorin DDH1 core
Beckers Fmn.	DMT 235.0	288.45	1.33	0.07	19.14	−24.27	5.44	Cranky Corner: Tangorin DDH1 core
Wasp Head Fmn.	LPB 1 — 0.1	287.32	0.42	0.04	9.56	−23.59	4.49	Depot Beach
Wasp Head Fmn.	LPB 2 — 0.2	287.23	4.97	0.21	24.22	−23.11	4.90	Depot Beach
Wasp Head Fmn.	LPB 5 — ALL	287.20	4.92	0.20	25.05	−23.08	4.46	Depot Beach
Wasp Head Fmn.	LPB 7 — 0.3	287.16	1.32	0.07	18.29	−23.26	4.49	Depot Beach
Wasp Head Fmn.	LPB 7 — 0.7	287.12	1.52	0.10	15.81	−22.67	4.05	Depot Beach
Wasp Head Fmn.	LPB 7 — 0.9	287.11	1.99	0.12	16.55	−22.65	3.98	Depot Beach
Wasp Head Fmn.	LPB 9 — 0.3	287.02	1.04	0.06	16.08	−23.39	4.49	Depot Beach
Lower Pebbley Beach Fmn.	LPB 10 — 0.2	286.97	2.16	0.10	21.77	−23.13	4.70	Depot Beach
Lower Pebbley Beach Fmn.	LPB 11 — 0.6	286.90	2.17	0.10	21.98	−23.33	4.56	Depot Beach
Lower Pebbley Beach Fmn.	LPB 12 — 0.1	286.88	2.90	0.14	20.99	−22.74	4.26	Depot Beach
Lower Pebbley Beach Fmn.	LPB 12 — 0.1R	286.88	3.00	0.14	21.69	−22.74	4.15	Depot Beach
Lower Pebbley Beach Fmn.	LPB 13 — 0.2	286.82	2.08	0.10	20.30	−22.99	3.94	Depot Beach
Lower Pebbley Beach Fmn.	LPB 14 — 0.1	286.81	2.94	0.14	21.40	−22.97	4.13	Depot Beach
Lower Pebbley Beach Fmn.	LPB 16 — 0.1	286.74	2.76	0.13	20.75	−22.90	3.61	Depot Beach
Lower Pebbley Beach Fmn.	LPB 16 — 0.5	286.69	2.90	0.13	23.18	−22.92	2.68	Depot Beach
Lower Pebbley Beach Fmn.	LPB 16 — 0.5A	286.69	11.44	0.31	36.68	−23.72	5.30	Depot Beach
Lower Pebbley Beach Fmn.	LPB 16 — 0.5B	286.69	15.85	0.43	36.64	−23.12	4.82	Depot Beach
Lower Pebbley Beach Fmn.	LPB 17 — 0.15	286.66	1.83	0.09	21.49	−23.38	3.12	Depot Beach
Lower Pebbley Beach Fmn.	LPB 18 — 0.9	286.54	2.02	0.11	18.70	−23.06	3.83	Depot Beach
Lower Pebbley Beach Fmn.	LPB 20 — 0.1	286.43	2.10	0.11	19.52	−22.95	3.64	Depot Beach
Lower Pebbley Beach Fmn.	LPB 20 — 1.1	286.30	2.22	0.11	19.43	−23.05	3.58	Depot Beach
Lower Pebbley Beach Fmn.	LPB 21 — 0.1	286.26	1.23	0.06	18.95	−23.01	2.89	Depot Beach
Lower Pebbley Beach Fmn.	LPB 22 — 0.3	286.21	2.42	0.13	18.69	−22.81	3.70	Depot Beach
Lower Pebbley Beach Fmn.	LPB 22 — 0.3R	286.21	2.45	0.13	19.04	−22.76	3.37	Depot Beach
Lower Pebbley Beach Fmn.	LPB 23 — 0.1	286.17	2.05	0.09	22.17	−23.18	3.97	Depot Beach
Lower Pebbley Beach Fmn.	LPB 24 — 0.4	286.10	2.50	0.12	20.45	−22.79	3.57	Depot Beach
Lower Pebbley Beach Fmn.	LPB 25 — 0.0	286.06	1.28	0.07	19.24	−22.86	3.60	Depot Beach
Lower Pebbley Beach Fmn.	LPB 25 — 0.5	286.00	1.73	0.10	17.73	−22.50	4.57	Depot Beach
Lower Pebbley Beach Fmn.	LPB-26 — 1.4	285.81	4.22	0.14	29.78	−22.94	3.88	Depot Beach
Lower Pebbley Beach Fmn.	LPB 27 — 0.2	285.78	2.56	0.14	18.64	−22.21	3.85	Depot Beach
Lower Pebbley Beach Fmn.	LPB 28 — 0.3	285.72	2.13	0.11	19.80	−22.38	4.12	Depot Beach
Lower Pebbley Beach Fmn.	LPB-28 — 0.55	285.69	3.46	0.09	39.59	−22.23	4.80	Depot Beach
Lower Pebbley Beach Fmn.	LPB 29 — 0.3	285.64	3.06	0.14	22.44	−22.30	3.65	Depot Beach
Lower Pebbley Beach Fmn.	LPB 29 — 0.5	285.61	3.07	0.14	21.82	−22.32	3.65	Depot Beach
Lower Pebbley Beach Fmn.	LPB 29 — 0.5R	285.61	3.21	0.14	22.54	−22.23	3.45	Depot Beach
Lower Pebbley Beach Fmn.	LPB 29 — 0.9	285.56	3.31	0.15	21.74	−22.22	3.57	Depot Beach
Lower Pebbley Beach Fmn.	LPB 31 — 0.1	285.53	2.72	0.14	19.66	−22.40	3.97	Depot Beach
Lower Pebbley Beach Fmn.	LPB 32 — 0.5	285.49	0.80	0.05	16.21	−22.70	4.16	Depot Beach
Lower Pebbley Beach Fmn.	LPB 33 — 0.0	285.48	3.40	0.15	22.52	−22.39	3.74	Depot Beach
Lower Pebbley Beach Fmn.	MPB 1 — 0.0	285.39	2.24	0.11	21.24	−22.27	4.56	Depot Beach
Lower Pebbley Beach Fmn.	LPB-35 — 0.0	285.39	4.19	0.15	27.76	−22.91	4.93	Depot Beach
Lower Pebbley Beach Fmn.	DLPB-35 — 0.0	285.39	4.22	0.15	28.23	−22.86	4.95	Depot Beach
Lower Pebbley Beach Fmn.	LPB 35 — 0.1	285.38	2.70	0.13	21.24	−22.46	4.03	Depot Beach
Lower Pebbley Beach Fmn.	LPB 36 — 0.0	285.36	0.96	0.05	18.09	−22.35	3.52	Depot Beach
Lower Pebbley Beach Fmn.	MPB 1 — 2.0	285.14	2.12	0.11	19.82	−22.37	4.03	Depot Beach
Lower Pebbley Beach Fmn.	UPB-0	285.07	1.65	0.08	19.46	−22.91	4.04	Depot Beach
Lower Pebbley Beach Fmn.	UPB-0R	285.07	1.66	0.08	19.73	−22.97	3.95	Depot Beach
Lower Pebbley Beach Fmn.	MPB 1 — 4.45	284.82	2.13	0.11	20.21	−22.51	4.08	Depot Beach
Lower Pebbley Beach Fmn.	MPB 2 — 1.0	284.68	1.49	0.09	16.33	−23.45	4.18	Depot Beach
Lower Pebbley Beach Fmn.	MPB 2 — 2.0	284.55	1.35	0.09	14.87	−23.48	4.66	Depot Beach
Lower Pebbley Beach Fmn.	MPB 3 — 0.4	284.48	2.04	0.09	23.09	−23.64	4.78	Depot Beach

Table 2. Results of geochemical analysis of Permian organic-rich facies from eastern Australia (continued).

Formation	Sample name	Age (Ma): Gradstein et al. (2004)	$\%C_{org}^{\diamond}$	$\%N_{total}^{\diamond}$	C_{org}/N_{total}	$\delta^{13}C_{org}$ (‰)*	$\delta^{15}N$ (‰)[†]	Locality
Lower Pebbley Beach Fmn.	MPB 3 — 1.0	284.40	2.67	0.12	22.74	−23.26	4.90	Depot Beach
Lower Pebbley Beach Fmn.	MPB 4 — 1.2	284.25	2.66	0.11	23.12	−22.64	4.08	Depot Beach
Lower Pebbley Beach Fmn.	MPB 4 — 2.8	284.04	2.30	0.10	22.67	−22.62	3.81	Depot Beach
Middle Pebbley Beach Fmn.	MPB 6 — 0.05	283.99	2.07	0.09	22.75	−22.73	4.01	Depot Beach
Middle Pebbley Beach Fmn.	DMPB 6 — 0.05	283.99	2.03	0.09	22.44	−22.71	4.42	Depot Beach
Middle Pebbley Beach Fmn.	MPB 6 — 0.9	283.85	2.25	0.10	22.78	−22.89	3.72	Depot Beach
Middle Pebbley Beach Fmn.	MPB 6 — 1.5	283.76	4.73	0.16	30.21	−22.99	3.73	Depot Beach
Middle Pebbley Beach Fmn.	MPB 6 — 2.25	283.64	2.09	0.09	24.01	−23.00	3.65	Depot Beach
Middle Pebbley Beach Fmn.	UPB-01	283.62	3.27	0.13	25.94	−22.72	3.48	Mill Point to Clear Point
Middle Pebbley Beach Fmn.	UPB-02	283.53	3.01	0.12	25.14	−22.67	3.55	Mill Point to Clear Point
Middle Pebbley Beach Fmn.	MPB 7 — 0.65	283.51	5.92	0.19	31.37	−23.27	3.67	Depot Beach
Middle Pebbley Beach Fmn.	MPB 7 — 1.30	283.40	3.47	0.11	30.58	−23.15	3.79	Depot Beach
Billy Brook Fmn.	DMT 152.70	283.32	1.14	0.06	20.37	−25.43	4.26	Cranky Corner: Tangorin core
Middle Pebbley Beach Fmn.	UPB-03	283.29	2.09	0.09	22.40	−23.02	3.78	Mill Point to Clear Point
Middle Pebbley Beach Fmn.	MPB 8 — 0.5	283.19	1.34	0.07	20.25	−22.29	3.83	Depot Beach
Billy Brook Fmn.	DMT 149.70	283.05	1.88	0.08	24.80	−24.85	5.67	Cranky Corner: Tangorin core
Middle Pebbley Beach Fmn.	MPB 9 — 1.3	282.98	1.74	0.08	22.56	−22.71	4.33	Depot Beach
Middle Pebbley Beach Fmn.	DMPB 9 — 1.3	282.98	1.76	0.08	23.01	−22.74	4.23	Depot Beach
Middle Pebbley Beach Fmn.	UPB-04	282.92	7.79	0.21	36.86	−23.01	3.76	Mill Point to Clear Point
Middle Pebbley Beach Fmn.	MPB 10 — 1.0	282.74	2.53	0.09	27.62	−22.49	3.83	Depot Beach
Billy Brook Fmn.	DMT 145.60	282.68	1.37	0.06	23.87	−24.75	4.45	Cranky Corner: Tangorin core
Billy Brook Fmn.	DMT 145.20	282.64	1.73	0.07	24.03	−24.76	4.45	Cranky Corner: Tangorin core
Middle Pebbley Beach Fmn.	UPB-05	282.56	3.53	0.12	29.03	−22.81	3.29	Mill Point to Clear Point
Upper Pebbley Beach Fmn.	UPB-06	282.45	1.92	0.08	22.82	−22.60	3.84	Mill Point to Clear Point
Billy Brook Fmn.	DMT 140.20	282.19	1.88	0.08	24.73	−24.47	4.01	Cranky Corner: Tangorin core
Fairyland Mbr., Buffel Fmn.	MUND-11 — 116.50	282.06	0.52	0.02	28.19	−26.69	10.37	Mundubbera-11 Core
Fairyland Mbr., Buffel Fmn.	MUND-11-115.10	282.01	0.70	0.02	32.20	−27.93	10.79	Mundubbera-11 Core
Billy Brook Fmn.	DMT 137.90	281.98	1.60	0.07	22.42	−24.53	4.45	Cranky Corner: Tangorin core
Fairyland Mbr., Buffel Fmn.	MUND-11-112.40	281.92	1.05	0.03	37.29	−24.89	8.17	Mundubbera-11 Core
Fairyland Mbr., Buffel Fmn.	MUND-11-110.40	281.85	0.47	0.02	25.74	−26.66	9.86	Mundubbera-11 Core
Fairyland Mbr., Buffel Fmn.	MUND-11-108.75	281.79	0.77	0.02	35.37	−24.58	7.63	Mundubbera-11 Core
Fairyland Mbr., Buffel Fmn.	MUND-11-107.52	281.75	0.32	0.01	21.73	−25.91	10.39	Mundubbera-11 Core
Fairyland Mbr., Buffel Fmn.	MUND-11-103.67	281.62	0.47	0.02	26.32	−25.66	9.54	Mundubbera-11 Core
Fairyland Mbr., Buffel Fmn.	DMUND-11-103.67	281.62	0.46	0.02	25.79	−25.72	9.67	Mundubbera-11 Core
Billy Brook Fmn.	DMT 131.20	281.37	1.38	0.07	19.95	−24.32	5.23	Cranky Corner: Tangorin core
Fairyland Mbr., Buffel Fmn.	MUND-11-95.28	281.33	0.67	0.02	29.00	−24.13	7.51	Mundubbera-11 Core
Fairyland Mbr., Buffel Fmn.	MUND-11-93.96	281.28	0.57	0.02	28.01	−24.46	8.18	Mundubbera-11 Core
Upper Pebbley Beach Fmn.	UPB-07	281.15	0.70	0.05	14.79	−22.80	4.28	Mill Point to Clear Point
Fairyland Mbr., Buffel Fmn.	MUND-11-89.80	281.14	0.67	0.02	27.11	−25.17	8.76	Mundubbera-11 Core
Fairyland Mbr., Buffel Fmn.	MUND-11-86.40	281.02	0.64	0.03	23.86	−26.13	10.76	Mundubbera-11 Core
Upper Pebbley Beach Fmn.	UPB-09	280.64	4.77	0.14	33.71	−23.04	3.36	Mill Point to Clear Point
Upper Pebbley Beach Fmn.	UPB-08	279.01	2.67	0.09	28.38	−23.22	3.88	Mill Point to Clear Point
Upper Pebbley Beach Fmn.	UPB-11	278.20	2.36	0.09	25.65	−23.49	−0.99	Mill Point to Clear Point
Upper Pebbley Beach Fmn.	UPB-14	277.15	0.77	0.07	11.67	−24.22	4.10	Mill Point to Clear Point
Upper Pebbley Beach Fmn.	UPB-15	276.38	3.29	0.11	29.87	−23.35	3.89	Mill Point to Clear Point
Upper Pebbley Beach Fmn.	UPB-16	276.06	2.19	0.09	25.21	−23.36	3.95	Mill Point to Clear Point
Snapper Point Fmn.	SP-07	275.40	3.29	0.12	27.01	−23.08	4.28	Pretty Beach
Snapper Point Fmn.	SP-06	275.19	1.31	0.06	22.48	−23.25	4.24	Snapper Point
Snapper Point Fmn.	DSP-06	275.19	1.31	0.06	22.49	−23.21	4.21	Snapper Point
Snapper Point Fmn.	SP-05	275.10	3.15	0.10	31.14	−23.88	5.31	Snapper Point
Snapper Point Fmn.	SP-04	275.10	7.79	0.20	38.39	−24.26	5.84	Snapper Point
Snapper Point Fmn.	SP-03	275.09	0.76	0.05	14.66	−23.30	4.60	Snapper Point
Snapper Point Fmn.	SP-02	275.09	3.82	0.14	27.99	−23.13	3.70	Snapper Point
Snapper Point Fmn.	SP-08	272.87	0.44	0.05	9.19	−23.70	6.30	Bannister's Point
Snapper Point Fmn.	SP-09	272.84	0.54	0.05	11.76	−23.48	6.37	Bannister's Point
Snapper Point Fmn.	SP-10	272.83	0.37	0.05	8.10	−23.86	6.67	Bannister's Point
Wandrawandian Siltstone	ECR 11- 178.65	272.46	0.37	0.03	13.09	−21.56	5.32	Elecom Clyde River-11 core
Wandrawandian Siltstone	ECR 11 — 174.8	272.42	0.43	0.02	18.29	−22.66	4.46	Elecom Clyde River-11 core
Wandrawandian Siltstone	ECR 11 — 167.38	272.33	0.87	0.06	14.58	−22.73	5.94	Elecom Clyde River-11 core
Wandrawandian Siltstone	ECR 11 — 162.45	272.27	0.97	0.07	14.77	−23.64	6.71	Elecom Clyde River-11 core
Wandrawandian Siltstone	ECR 11 — 145.3	272.07	0.22	0.02	9.54	−23.06	5.37	Elecom Clyde River-11 core
Wandrawandian Siltstone	ECR 11 — 134.95	271.95	0.59	0.04	15.56	−22.99	5.21	Elecom Clyde River-11 core
Wandrawandian Siltstone	ECR 11 — 126.17	271.85	1.12	0.07	15.34	−23.17	4.71	Elecom Clyde River-11 core
Wandrawandian Siltstone	ECR 11 — 116.14	271.73	0.38	0.04	10.57	−23.50	5.50	Elecom Clyde River-11 core
Wandrawandian Siltstone	ECR 11 — 104.4	271.59	1.07	0.06	18.17	−23.29	5.91	Elecom Clyde River-11 core
Wandrawandian Siltstone	ECR 11 — 97.7	271.51	1.34	0.07	19.10	−23.13	5.25	Elecom Clyde River-11 core
Wandrawandian Siltstone	ECR 11 — 93.8	271.47	1.19	0.07	17.19	−22.87	5.02	Elecom Clyde River-11 core
Wandrawandian Siltstone	ECR 11 — 82.86	271.34	2.75	0.12	23.54	−25.19	3.67	Elecom Clyde River-11 core
Wandrawandian Siltstone	ECR 11 — 55.53	271.02	1.73	0.11	15.62	−23.59	7.12	Elecom Clyde River-11 core
Wandrawandian Siltstone	ECR 11 — 42.94	270.87	0.87	0.07	12.57	−24.05	7.43	Elecom Clyde River-11 core
Erins Vale Fmn.	BUN 1251.00	266.90	0.70	0.09	8.15	−23.30	8.22	Pacific Power Bunnerong Core, Sydney
Erins Vale Fmn.	BUN 1241.70	266.83	1.50	0.15	9.91	−24.19	7.22	Pacific Power Bunnerong Core, Sydney
Erins Vale Fmn.	BUN 1230.05	266.73	1.08	0.15	7.06	−23.95	7.40	Pacific Power Bunnerong Core, Sydney
Erins Vale Fmn.	BUN 1220.30	266.65	1.65	0.16	10.23	−23.79	6.62	Pacific Power Bunnerong Core, Sydney
Erins Vale Fmn.	BUN 1217.25	266.63	1.14	0.12	9.22	−23.94	6.54	Pacific Power Bunnerong Core, Sydney
Erins Vale Fmn.	BUN 1209.77	266.57	0.83	0.12	7.14	−24.12	6.69	Pacific Power Bunnerong Core, Sydney
Erins Vale Fmn.	BUN 1192.42	266.43	1.65	0.18	9.16	−23.25	4.47	Pacific Power Bunnerong Core, Sydney
Wilton Fmn.	BUN 1172.47	266.12	0.93	0.09	10.74	−23.51	4.92	Pacific Power Bunnerong Core, Sydney
Wilton Fmn.	BUN 1162.40	265.63	1.65	0.13	12.63	−23.36	4.27	Pacific Power Bunnerong Core, Sydney

Table 2. Results of geochemical analysis of Permian organic-rich facies from eastern Australia (continued).

Formation	Sample name	Age (Ma): Gradstein et al. (2004)	%$C_{org}$$^\diamond$	%$N_{total}$$^\diamond$	C_{org}/N_{total}	$\delta^{13}C_{org}$ (‰)*	$\delta^{15}N$ (‰)†	Locality
Wilton Fmn.	BUN 1151.00	265.08	1.58	0.18	8.56	−23.48	4.09	Pacific Power Bunnerong Core, Sydney
Wilton Fmn.	DBUN 1151.00	265.08	1.61	0.19	8.61	−23.47	4.27	Pacific Power Bunnerong Core, Sydney
Wilton Fmn.	BUN 1139.15	264.50	3.58	0.22	16.65	−24.64	1.65	Pacific Power Bunnerong Core, Sydney
Wilton Fmn.	BUN 1129.50	264.03	1.89	0.17	11.09	−24.68	2.64	Pacific Power Bunnerong Core, Sydney
Wilton Fmn.	BUN 1121.76	263.65	0.70	0.20	3.55	−24.81	2.31	Pacific Power Bunnerong Core, Sydney
Wilton Fmn.	BUN 1105.74	262.88	2.34	0.15	15.16	−24.67	2.42	Pacific Power Bunnerong Core, Sydney
Wilton Fmn.	BUN 1094.90	262.35	1.30	0.14	9.03	−24.45	2.03	Pacific Power Bunnerong Core, Sydney
Wilton Fmn.	BUN 1082.50	261.74	0.53	0.20	2.62	−24.80	2.87	Pacific Power Bunnerong Core, Sydney
Bargo Claystone	BUN 1065.00	260.97	2.70	0.14	19.00	−24.64	2.65	Pacific Power Bunnerong Core, Sydney
Bargo Claystone	BUN 1055.18	260.85	2.88	0.15	18.92	−24.58	2.63	Pacific Power Bunnerong Core, Sydney
Bargo Claystone	BUN 1045.70	260.73	2.04	0.22	9.31	−24.48	2.63	Pacific Power Bunnerong Core, Sydney
Bargo Claystone	BUN 1034.30	260.58	3.09	0.17	18.36	−24.44	2.61	Pacific Power Bunnerong Core, Sydney
Bargo Claystone	DBUN 1034.30	260.58	3.09	0.17	18.38	−24.44	2.54	Pacific Power Bunnerong Core, Sydney
Bargo Claystone	BUN 1022.70	260.44	1.80	0.13	13.42	−24.54	2.74	Pacific Power Bunnerong Core, Sydney
Bargo Claystone	BUN 1014.70	260.33	1.49	0.13	11.57	−24.35	2.88	Pacific Power Bunnerong Core, Sydney
Bargo Claystone	BUN 1005.56	260.22	1.02	0.11	9.09	−24.11	3.00	Pacific Power Bunnerong Core, Sydney
Bargo Claystone	BUN 998.65	260.13	0.92	0.11	8.13	−23.92	3.07	Pacific Power Bunnerong Core, Sydney
Bargo Claystone	BUN 996.34	260.10	1.42	0.12	12.27	−23.78	3.08	Pacific Power Bunnerong Core, Sydney

*$\delta^{13}C_{org}$ values reported in per mil (‰) relative to Vienna Peedee Belemnite standard (V-PDB).
†$\delta^{15}N$ values reported in per mil (‰) relative to AIR standard.
$^\diamond$% C$_{org}$ and %N$_{total}$ reported in weight percent (wt.%).

5.2. Controls on $\delta^{13}C_{org}$

5.2.1. Local-scale controls

Because organic matter source is variable throughout the succession, changes in the ratio of terrestrial to marine organic matter play a role in determining the nature and extent of temporal shifts in $\delta^{13}C_{org}$ values. For instance, the negative excursion at the end of P2 (early Artinskian) is enhanced because this part of the curve is defined by data from the Fairyland Member of the Dresden Formation, which contains more terrestrially derived organic matter ($C_{org}/N_{tot} \geq 21.73$) than do enclosing formations (Figure 4a). However, several aspects of the dataset suggest that temporal variations in $\delta^{13}C_{org}$ are caused by factors unrelated to organic matter source. For example, if the main control on temporal variations in $\delta^{13}C_{org}$ were organic matter source, then one would expect a strong correlation between C_{org}/N_{tot} and $\delta^{13}C_{org}$. This is not the case. Rather, the correlation between these variables is weak ($r^2 = 0.04$; Figure 3a). Moreover, in the lower Pebbley Beach Formation, large pieces of fossil wood were sampled and analyzed for C_{org}/N_{tot} and $\delta^{13}C_{org}$. In general, the C_{org}/N_{tot} ratios returned for these wood samples are elevated (avg. = 33.1, $n = 6$) compared to bulk organic matter from the same formation (avg. = 20.4, $n = 30$), reflecting the fully terrestrial origin of the fossil wood. However, the average $\delta^{13}C_{org}$ values of the fossil wood (23‰) are virtually indistinguishable from those of the bulk organic matter (22.7‰). Considering only data with C_{org}/N_{tot} values > 20, or fully terrestrial organic matter, the resulting curve displays the same positive and negative, A and B, $\delta^{13}C_{org}$ shifts that are displayed using the total dataset (Figure 5b).

Other environmental factors, such as water stress, have been shown to influence the $\delta^{13}C_{plant}$ values, with reduced water availability and increased water-use efficiency resulting in more positive $\delta^{13}C_{org}$ values (Gröcke, 1998). By inference, $\delta^{13}C_{org}$ values of terrestrial bulk organic matter react similarly (Montañez et al., 2007). As such, temporal or interbasinal changes in water availability in eastern Australia may have caused $\delta^{13}C_{org}$ shifts exhibited in the $\delta^{13}C_{org}$ curve in Figure 4b. Interbasinal variations in $\delta^{13}C_{org}$ are apparent, as illustrated in Figure 5. $\delta^{13}C_{org}$ values from the Fairyland Member (Bowen Basin) and Billy Brook and Beckers Formations (Cranky Corner) are more negative than those from the Sydney Basin, resulting in higher magnitude $\delta^{13}C_{org}$ shifts in the overall composite record from Eastern Australia, and suggesting the Bowen Basin (Fairyland Member) and Cranky Corner region were wetter than the Sydney Ba-sin. Despite interbasinal environmental variations, note similar $\delta^{13}C_{org}$ directional shifts (A–F) remain when data from the Sydney Basin are plotted alone (Figure 5a).

5.2.2. Global-scale controls

Because 1) $\delta^{13}C_{org}$ shifts cannot be attributed entirely to changes in organic matter source and/or environmental conditions, 2) samples can be directly tied to climatic interpretations made from sedimentologic observations from the same succession, and 3) $\delta^{13}C_{org}$ shifts occur in concordance with P2–P4 glacial intervals documented from same region, $\delta^{13}C_{org}$ shifts A–F are interpreted to reflect climate-related changes in carbon cycling in both the terrestrial and marine environment. Shifts in $\delta^{13}C_{org}$ of terrestrial organic matter, or more specifically modern plants and ancient fossil wood and plants, have been shown to record changes in atmospheric pCO$_2$, and/or changes in the isotopic composition of atmospheric CO$_2$ ($\delta^{13}C_a$) (Keeling et al., 1979; Marino & McElroy, 1991; Gröcke et al., 1999; Arens et al., 2000; Gröcke, 2002). Since studies have recognized a covariance between glaciation and pCO$_2$ levels during the late Paleozoic (Royer et al., 2004; Montañez et al., 2007), it is logical that the $\delta^{13}C_{org}$ values of terrestrial organic matter would reflect climatically-related pCO$_2$ changes in concert with the glacial sedimentologic and stratigraphic record. Because the earlier portion of the $\delta^{13}C_{org}$ record (pre-mid-Kungurian, shifts A and B during P2 glacial interval) reflects a more terrestrial organic matter source and the later portion of the record (post-mid-Kungurian, shifts C, D, E, and F during P3 and P4 glacial intervals) reflects a more mixed terrestrial and marine organic matter source (Figure 4), the behaviour of $\delta^{13}C_{org}$ values in the marine realm must also be considered. Note that shifts C, D, E, and F during glacial intervals P3 and P4, though more modest, are similar in direction to shifts A and B during glacial interval P2. This suggests the marine and terrestrial realm responded similarly to changes in carbon cycling associated with climatic changes. We interpret changes in $\delta^{13}C_{org}$ value of marine organic matter to be a result of changes in oceanic productivity and/or changes in oceanic and continental organic matter burial that drove or acted in harmony with changes in pCO$_2$ and $\delta^{13}C_a$, which affected the $\delta^{13}C_{org}$ value of terrestrial organic matter. In other words, increased organic matter burial resulted in an increase in the $\delta^{13}C_{org}$ value of marine organic matter, a drawdown in atmospheric pCO$_2$, and an increase in $\delta^{13}C_{org}$ value of terrestrial organic matter. In accordance with these models of isotopic behaviour and recognizing
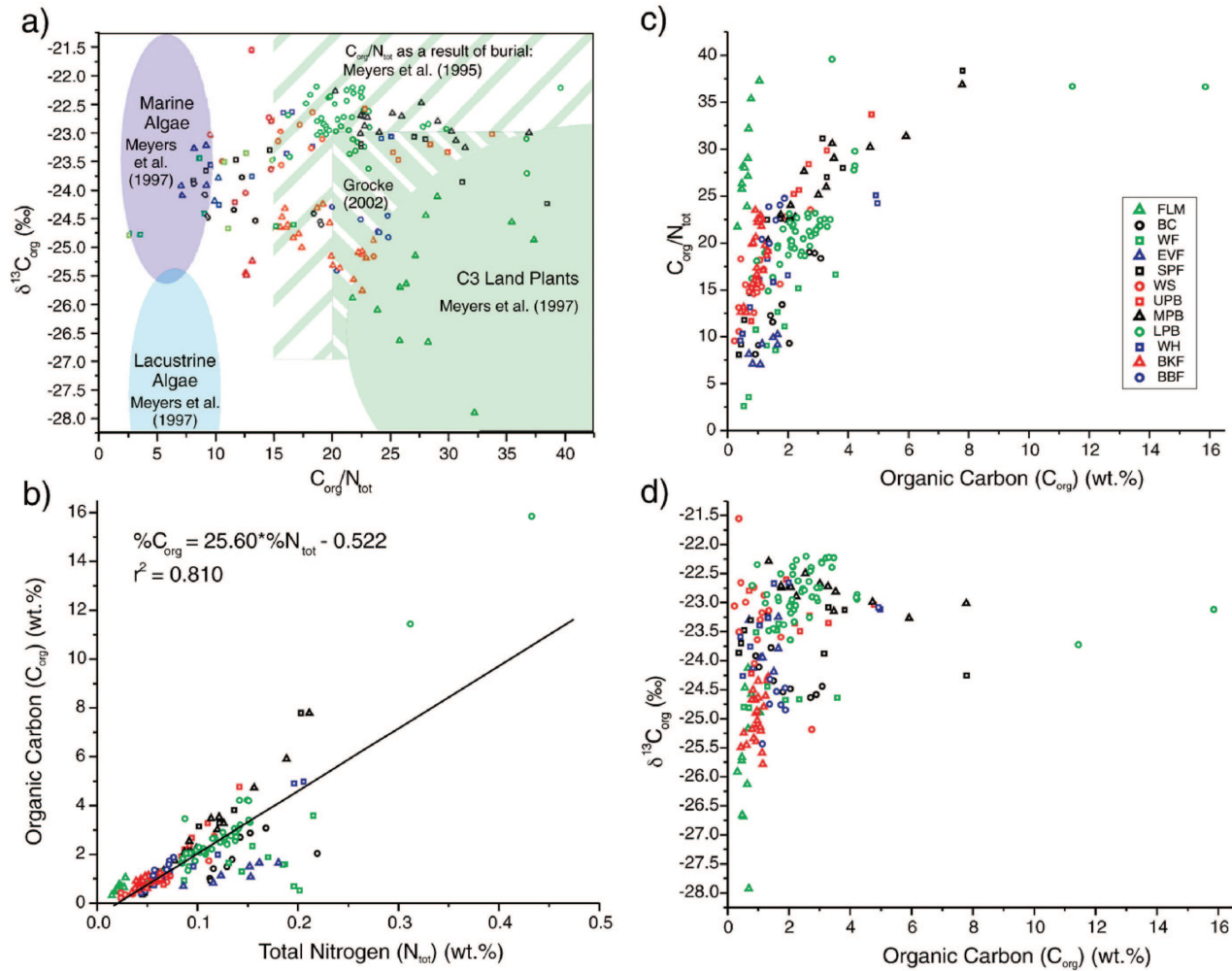
Figure 3. Crossplots of total organic carbon content (% C_{org}), total nitrogen content (% N_{tot}), C_{org}/N_{tot}, and $\delta^{13}C_{org}$ data obtained from analysis of 175 Permian organic-rich sediment samples, plotted by formation. $\delta^{13}C_{org}$ data reported in per mil (‰) relative to Vienna Pee Dee Belemnite (V-PDB). **a)** $\delta^{13}C_{org}$ vs. C_{org}/N_{tot}, $r^2 = 0.04$. Plotted fields are based on Meyers (1997) and Gröcke (2002). b) % C_{org} vs. % N_{tot}, $r^2 = 0.810$. c) C_{org}/N_{tot} vs. % C_{org}, $r^2 = 0.56$. d) $\delta^{13}C_{org}$ versus % C_{org}., $r^2 = 0.30$.

that positive $\delta^{13}C_{org}$ shifts A, C, and E record the onset of glacial intervals P2–P4, we interpret positive $\delta^{13}C_{org}$ shifts A, C, and E to record a decrease in pCO_2 and/or an increase in $\delta^{13}C_a$ in the terrestrial realm and an increase in organic matter burial in the marine realm. Conversely, we interpret negative $\delta^{13}C_{org}$ shifts B, D, and F that occur during the middle to end of glacial intervals P2–P4, to record deglaciation along with a concomitant rise in pCO_2 and/or an increase in $\delta^{13}C_a$ in the terrestrial realm and a decrease in organic matter burial in the marine realm.

The larger magnitude of shifts A and B during P2 relative to shifts C, D, E, and F during P3 and P4 reflects the overall transition from the peak to waning stages of the icehouse, as documented by Fielding et al. (2008a, 2008b, 2008c), Isbell et al. (2003), and Montañez et al. (2007). Evidence for post-Sakmarian glacial conditions or glacial intervals P3 and P4 is limited to eastern Australia and Siberia, suggesting glaciation across most of Gondwana ended during the Sakmarian, with limited lingering regional glaciation (Domack et al., 1993; Chumakov, 1994; Isbell et al., 2003; Fielding et al., 2008a, 2008c). The progressive decrease in the magnitude of $\delta^{13}C_{org}$ shifts supports this global climate view.

5.3. Pebbley Beach Formation

The Pebbley Beach Formation provides one example of how interpreted relationships between $\delta^{13}C_{org}$ and climatically related

changes in pCO_2 can be directly tied and supported by climatic interpretations made from sedimentologic and stratigraphic observations within the formation and interpretations of global climate patterns. The formation contains independent sedimentologic and stratigraphic evidence for climate change within glacial interval P2, the most widespread of the glacial intervals, recording successively 1) regional maximum glacial extent in the lower member, 2) deglaciation in the middle member, and 3) glacioeustatic effects from distant glaciers during the waning stages of P2 in the upper member (Figure 6; see Fielding et al., 2006, 2008b] for detailed sedimentologic documentation and interpretation). The lower member contains the most direct evidence of glaciation, consisting of cyclic alternations between diamictite and siltstone, bound by a hiatal surface, and is interpreted to record repeated glacial advance and retreat (Fielding et al., 2008b). The middle member contains sparse outsized clasts that tend to occur within discrete horizons, which indicates episodic presence of floating ice and the overall retreat of glaciers from the region during deposition (Fielding et al., 2008b). Finally, the upper member contains no evidence for nearby glacial activity or floating ice, but does contain several sequences that suggest sea level varied by ~ 50–70 m during deposition as a result of isostatic loading from a nearby glacier (Figure 6; Fielding et al., 2006, 2008b). The underlying Wasp Head Formation (Rygel et al., 2008; Fielding et al., 2008b) and overlying Snapper Point Formation (Rygel et al., 2008;

Figure 4. a) C_{org}/N_{tot} and **b)** $\delta^{13}C_{org}$ versus Permian time for eastern Australia dataset. Interpretations of directional data shifts plotted to left. Noted positive $\delta^{13}C_{org}$ shifts coincident with the onset of glacial episodes P2–P4 include A, C, E. Noted negative $\delta^{13}C_{org}$ shifts during the middle to end of glacial episodes P2–P4 include B, D, F.
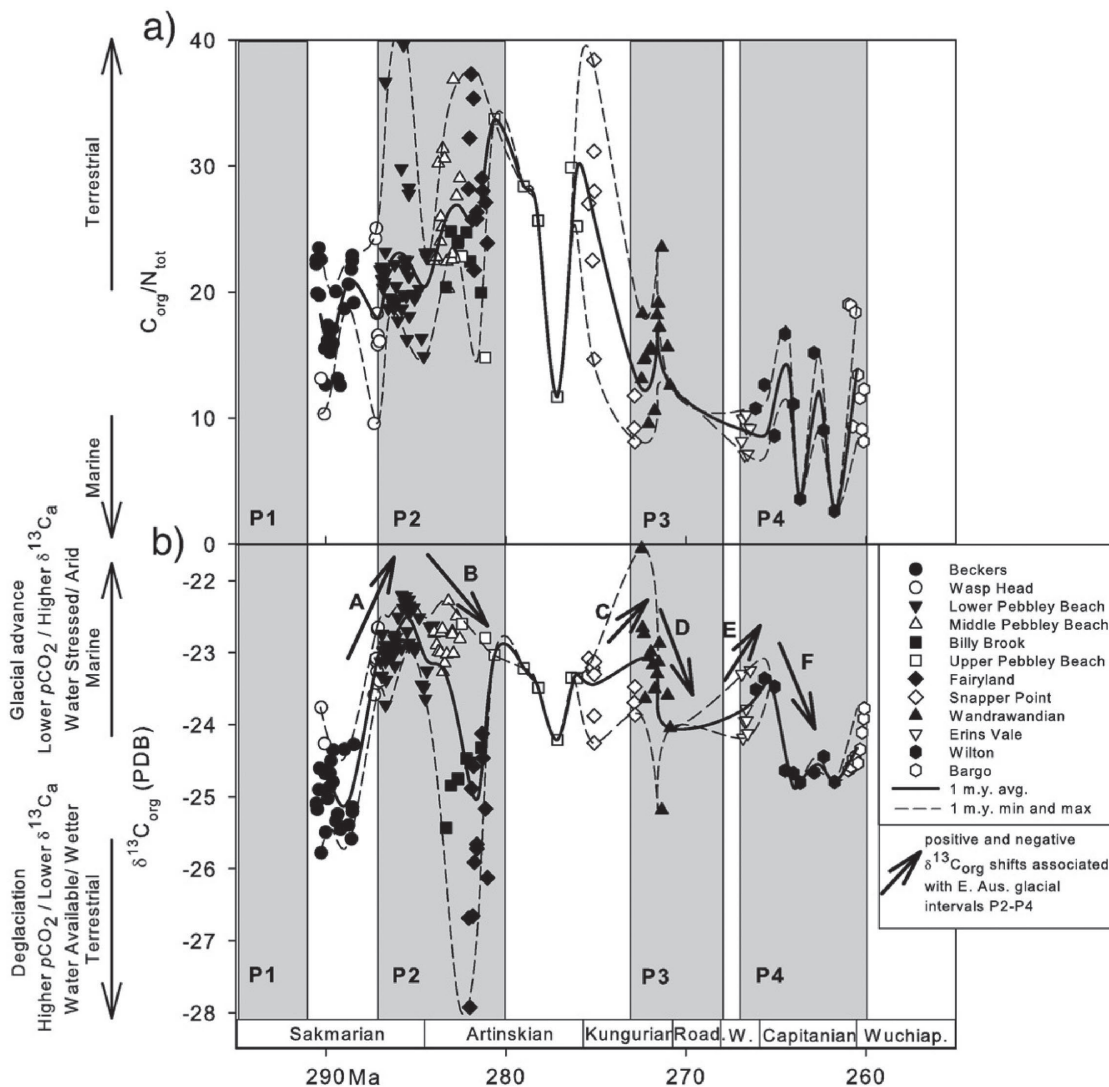
Bann et al., 2008) are interpreted to record nonglacial conditions preceding and succeeding glacial episode P2, respectively (Fielding et al., 2006, 2008b).

Figure 6 illustrates the relationships between $\delta^{13}C_{org}$ and the sedimentary record of the Pebbley Beach Formation. The lower Pebbley Beach Formation, the member that contains direct evidence of glaciation, is associated with a positive shift in $\delta^{13}C_{org}$, suggesting a drop in pCO_2 and/or an increase in $\delta^{13}C_a$ and cooling associated with the peak glacial conditions recorded within the formation and/or glacial advance. Two declines in $\delta^{13}C_{org}$ follow. The first decrease in $\delta^{13}C_{org}$ occurs at the top of the lower Pebbley Beach Formation (magnitude 1.25‰), in association with the last diamictite unit. The excursion is brief with values quickly returning to more moderate values in the middle Pebbley Beach Formation, perhaps illustrating a brief retreat of glacial conditions near the top of the lower Pebbley Beach Formation, as the last diamictite unit records a significant deglaciation phase. The second, more gradual decline in $\delta^{13}C_{org}$ occurs through the middle and upper Pebbley Beach Formation (magnitude 2.35‰), synchronous with the amelioration of climate and overall glacial retreat documented in the sedimentary record (Figure 6). In the Pebbley Beach Formation, the correspondence between facies changes and the shifts in $\delta^{13}C_{org}$ support the interpretation that $\delta^{13}C_{org}$ reflects changes in climate related to changes in atmospheric CO_2 (Figure 6).

5.4. Comparison to other proxy records

5.4.1. $\delta^{13}C$ records

The recognition of global-scale controls on the $\delta^{13}C_{org}$ curve constructed from eastern Australia is further supported by comparison to other geochemical proxy datasets, particularly during the most widespread of the glacial intervals, P2 (Figure 7). Comparison of the eastern Australian $\delta^{13}C_{org}$ curve with terrestrial $\delta^{13}C_{org}$ curves constructed from paleoequatorial latitudes, namely from North China coals and from fossil plant and bulk organic matter from mid-continent localities of the U.S. (Zhang et al., 1999; Montañez et al., 2007), reveals a similar positive followed by a negative $\delta^{13}C_{org}$ shift during glacial interval P2 (Figure 7c). This covariance in widely-dispersed geochemical datasets confirms that 1) glacial interval P2 is one of global extent and is recorded in the $\delta^{13}C_{org}$ record worldwide, as indicated by Montañez et al. (2007), and 2) $\delta^{13}C_{org}$ shifts A and B (during P2) from the eastern Australian record are primarily controlled by global-scale variables such as changes in pCO_2, $\delta^{13}C_a$, and organic matter burial, rather than local changes in organic matter source and environmental variables. $\delta^{13}C_{org}$ shifts C, D, E, and F from eastern Australia during glacial intervals P3 and P4 are not apparent in other $\delta^{13}C_{org}$ datasets, likely due to a combination of factors (Figure 7). Firstly, the Montañez et al. (2007) dataset does not continue beyond the onset of P3 (Figure 7c). Sec-

Figure 5. a) $\delta^{13}C_{org}$ versus Permian time. Plotted datapoints from the Sydney Basin only. **b)** $\delta^{13}C_{org}$ versus Permian time. All plotted datapoints exhibit fully terrestrial organic matter source, as indicated by $C_{org}/N_{tot} > 20$. **c)** Total eastern Australian dataset ($\delta^{13}C_{org}$ versus Permian time) for reference, as shown in Figure 4b. Interpretations of directional data shifts plotted to left. All $\delta^{13}C_{org}$ data reported in per mil (‰) relative to Vienna Pee Dee Belemnite (V-PDB).
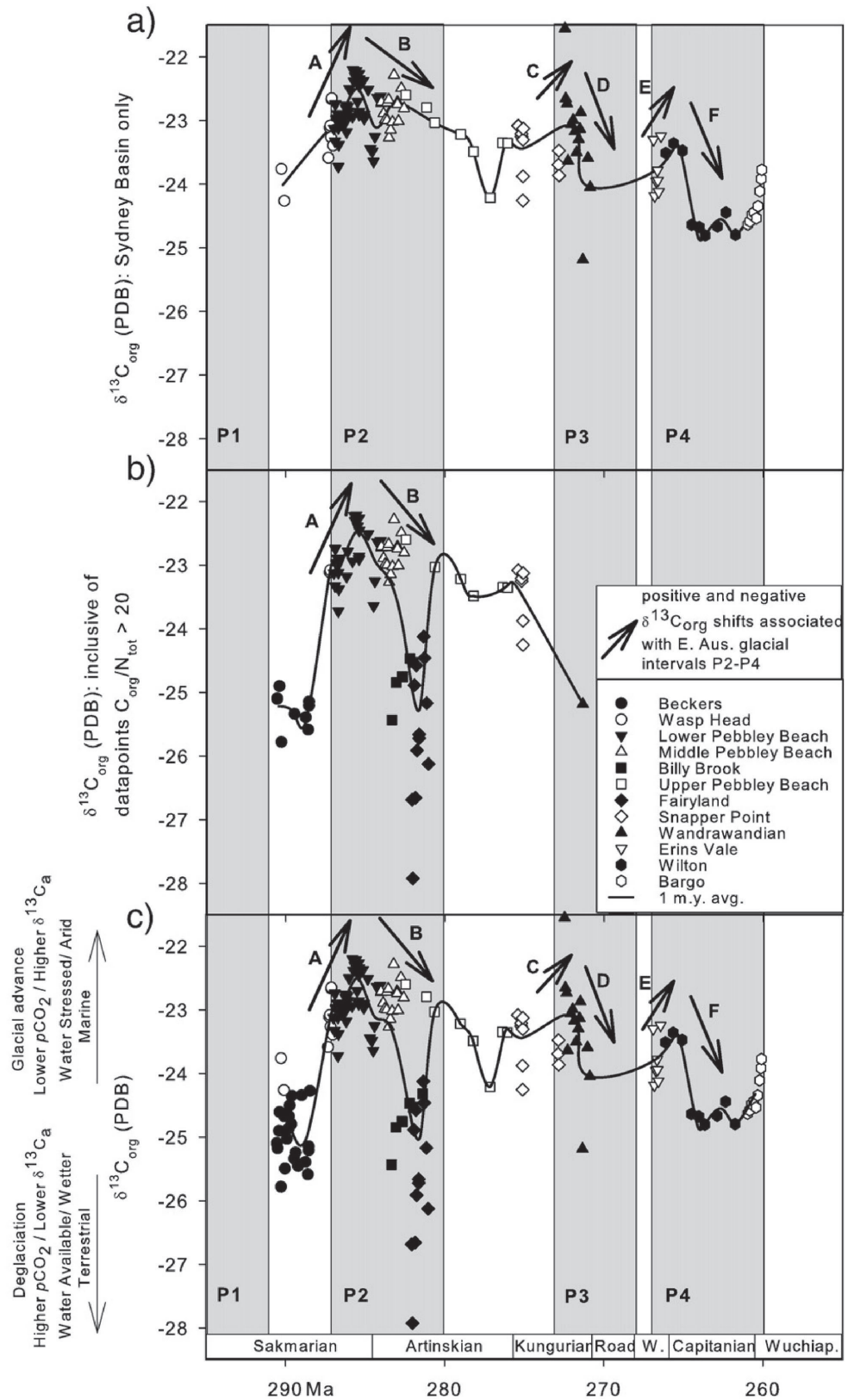
ondly, a positive $\delta^{13}C_{org}$ shift in the Zhang et al. (1999) dataset just prior to P3 may actually be recording the onset of glacial interval P3, but the apparent offset is a result of poor cross-latitudinal correlation of datasets (Figure 7c). Alternatively, climatic variations associated with glacial intervals P3 and P4 are not recorded in the Zhang et al. (1999) dataset because 1) the Zhang

et al. (1999) dataset records an overall decline in $\delta^{13}C_{org}$ values associated with the longer-term transition from icehouse to greenhouse conditions rather than individual shorter-term glacial intervals P3–P4 recorded in eastern Australia, 2) glaciation during P3 and P4 was restricted to eastern Australia and Siberia, as suggested by current models of the late Paleozoic ice age
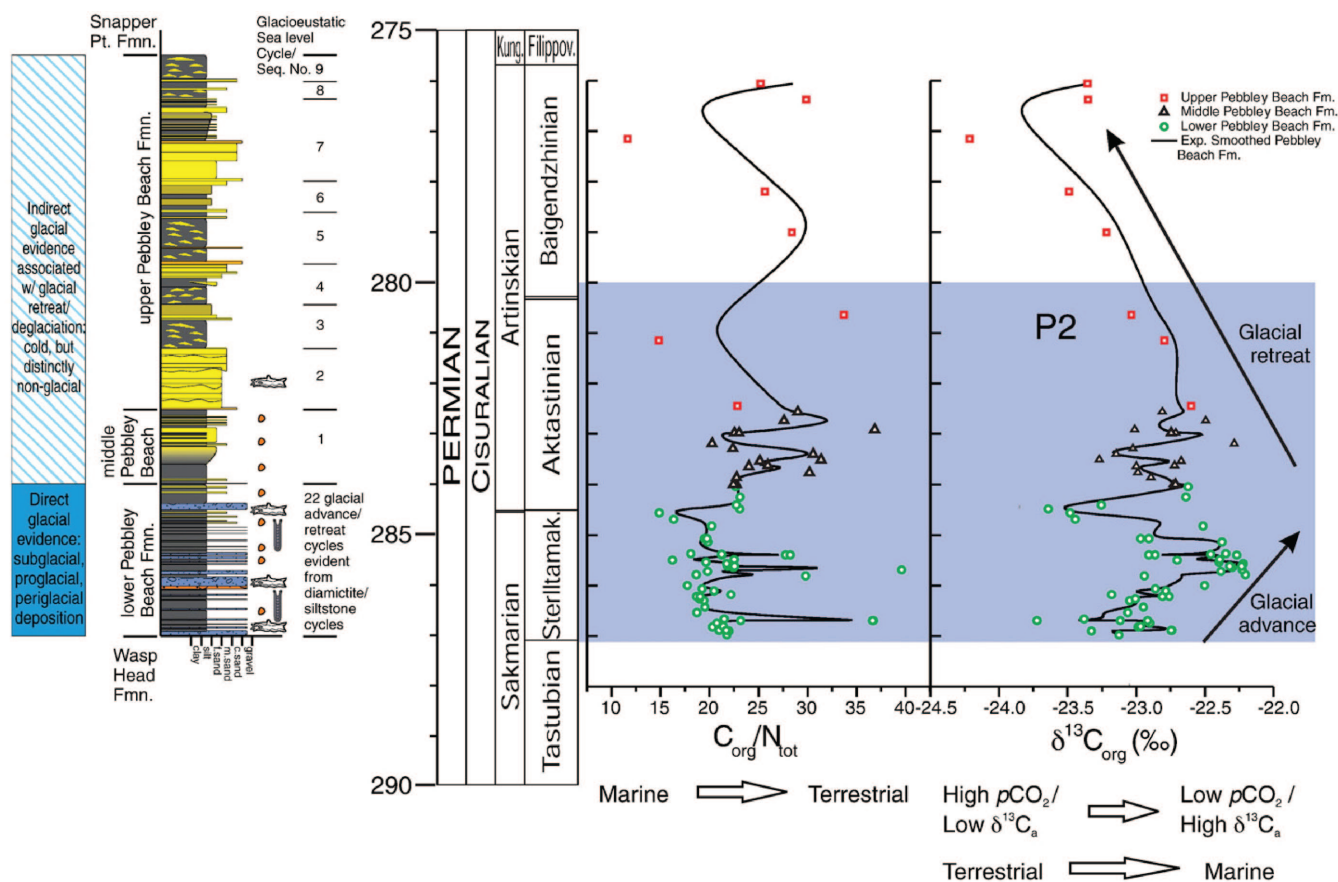
Figure 6. Examination of parallel relationships between environmental/climatic interpretations based on sedimentologic and stratigraphic field relationships (left) and climatic/pCO$_2$ interpretations based on geochemical organic carbon isotopic data from the Pebbley Beach Formation (right). Note C_{org}/N_{tot} values suggest a largely terrestrial source, with some minor marine influence. Peaks in C_{org}/N_{tot} are, in some cases, based on one value and do not represent the system overall.

(Fielding et al., 2008a, 2008c), and not reflected in $\delta^{13}C_{org}$ datasets across the globe, or 3) environmental or dominant-maceral composition changes on the North China platform exert a primary control on the latter portion of the Zhang et al. (1999) $\delta^{13}C_{org}$ curve.

Comparable isotopic records that span the Permian and are derived from well-preserved brachiopod calcite are few (Veizer et al., 1999; Korte et al., 2005) and of too low a resolution to facilitate direct comparison to the organic matter record presented here (Figure 7b). Figure 7b illustrates the $\delta^{13}C_{carb}$ datasets of Veizer et al. (1999) and Korte et al. (2005), as presented by Montañez et al. (2007) and Frank et al. (2008) after careful data screening for diagentic effects and conversion of data points to the Gradstein et al. (2004) timescale (see Frank et al. 2008 for details). Future research efforts should be aimed at resolving the $\delta^{13}C_{carb}$ record through the Permian.

However, recently, paleoequatorial $\delta^{13}C_{carb}$ and fossil records have been constructed from a shorter time interval, spanning the late Wordian, Capitanian, and early Wuchiapingian (e.g. Isozaki et al., 2007a, 2007b). These records document a 3–4 million-year, early Capitanian cooling event, evidenced by a period of elevated $\delta^{13}C_{carb}$ values, thought to reflect increased marine productivity and pCO$_2$ drawdown (Isozaki et al., 2007a, 2007b). This cooling event is associated with the end-Guadalupian (Capitanian) extinction event, and, specifically, extinction of gigantic bivalves is thought to have been caused by cooling in tropical seas during this time (Isozaki and Aljinovic, 2009). The timing of glacial episode P4, based on sedimentary evidence in Eastern Australia (Fielding et al., 2008a, 2008b), is roughly coeval with this

early Capitanian cooling event (Figure 4, Figure 5, and Figure 7), within error of cross-latitudinal age comparison. $\delta^{13}C_{org}$ shift E, interpreted to record the onset of glacial episode P4, may coincide with the onset of a period of elevated $\delta^{13}C_{carb}$ values (cooling event) from the tropical realm.

5.4.2. Paleosol-derived pCO₂ reconstruction

Atmospheric pCO$_2$ data calculated from the $\delta^{13}C$ values of paleosol carbonate and goethite from Royer (2006) display relatively low values during P1, P2, and P3 glacial intervals, with a marked increase between P2 and P3 and during P4 glacial interval (Figure 7a). Paleosol-derived values of pCO$_2$ begin low and are roughly concurrent with a positive $\delta^{13}C_{org}$ shift A from the eastern Australian record (interpreted as a drop in pCO$_2$ and/or an increase in $\delta^{13}C_a$). Additionally, pCO$_2$ values rise in the mid-Artinskian near the end of glacial episode P2, which is roughly coeval with the negative $\delta^{13}C_{org}$ shift B from the eastern Australian record (Figure 7a, d). A mid-Artinskian through mid-Kungurian period of relatively higher pCO$_2$ values corresponds to a period that lacks sedimentary evidence for glacial processes in eastern Australia and also Antarctica (Montañez et al., 2007). A positive $\delta^{13}C_{org}$ shift at the base of P3, shift C, slightly precedes a drop in pCO$_2$ recorded from paleoequatorial paleosols (Figure 7a, d). The offset in timing of the events may reflect difficulties in correlating datasets from different hemispheres and/ or differences in dataset resolution. Relatively high paleosol-derived pCO$_2$ values during glacial interval P4 is consistent with other global trends of overall warming with lingering regional ice-influence in eastern Australia.

Figure 7. Comparison of paleoequatorial proxy datasets to $\delta^{13}C_{org}$, eastern Australian dataset presented herein. **a)** Reconstructed pCO_2 (best, maximum and minimum estimate according to Royer, 2006), as estimated from $\delta^{13}C$ of paleosol carbonate nodules and stomatal indices (Royer, 2006). **b)** $\delta^{13}C_{carb}$ data from low-Mg calcite, non-luminescent brachiopod shells from Veizer et al. (1999) and Korte et al. (2005), as presented by Montañez et al. (2007) and Frank et al. (2008) after careful data screening and conversion of data points to Gradstein et al. (2004) timescale. Criteria for data screening to only include low-Mg calcite, non-luminescent brachiopod shells explained in detail in Frank et al. (2008). Trendlines plotted using 1 m.y. average values of the dataset. c) $\delta^{13}C_{org}$ datasets of Montañez et al. (2007), constructed from fossil plant matter collected from the Anadarko, Pedregosa, and the Eastern Shelf of the Midlands Basin, and Zhang et al. (1999), constructed from coals from the North China Platform. Trendlines plotted using 1 m.y. average values of the dataset. Montañez et al. (2007): "c and p" represents all compression and permineralized plant matter, coal, and charcoal samples.
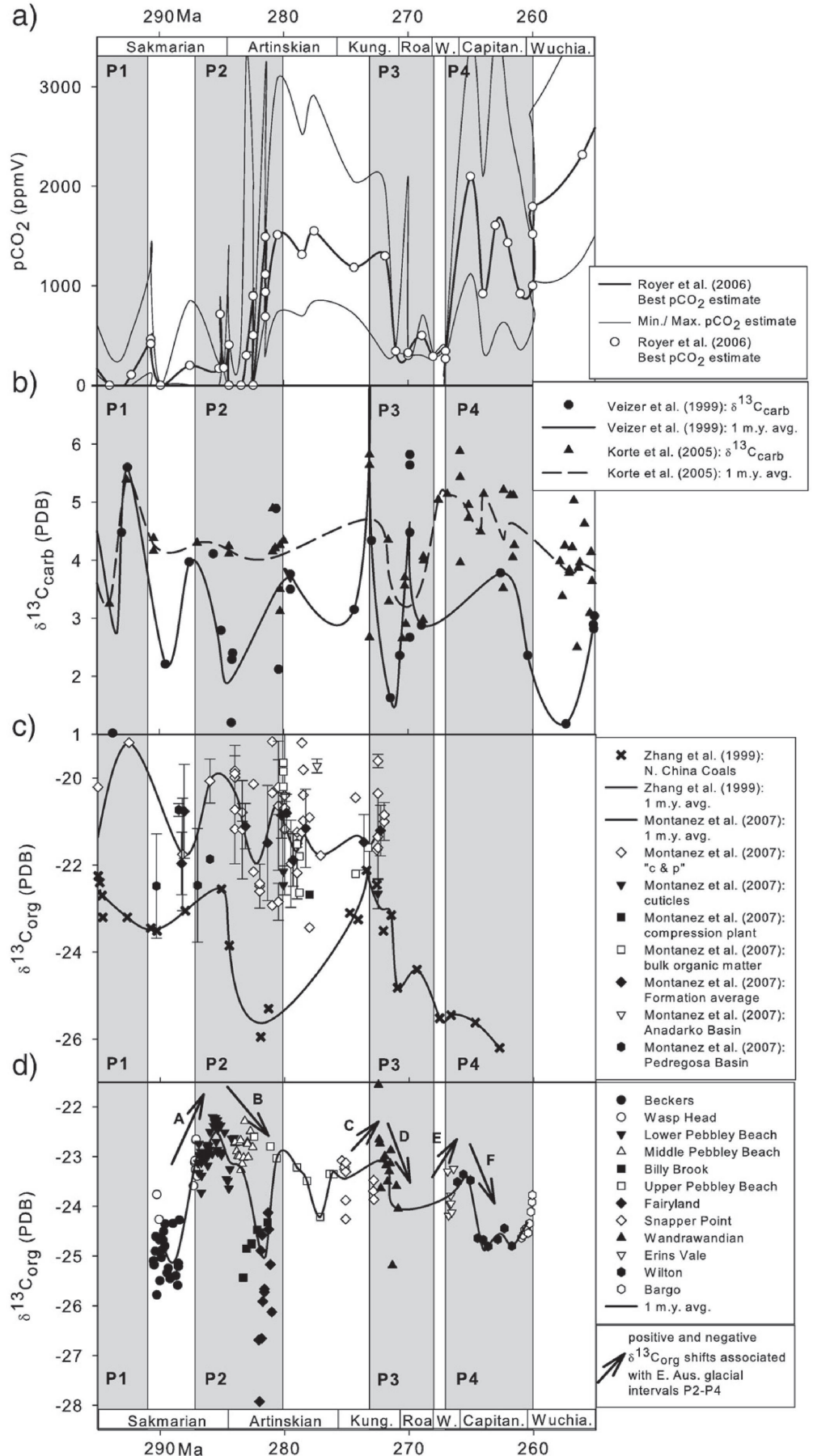
6. Implications

Because the $\delta^{13}C_{org}$ record was sampled from a highly resolved, high-latitude record of Permian glaciation, relationships between $\delta^{13}C_{org}$ and climate documented herein can be used as a model for further investigations of late Paleozoic climate, particularly in studies that seek to link paleoequatorial proxies to Gondwanan records. Investigation of the Permian $\delta^{13}C_{org}$ record from eastern Australia supports the dynamic nature of climatic variability documented the sedimentary record of glaciation from eastern Australia, namely that glacial (P2–P4) and nonglacial conditions alternated on ~ 5–7 m.y. timescales amidst an overall transition from the peak to the waning stages of icehouse conditions (Fielding et al., 2008a, 2008b). Furthermore, this study demonstrates a broad covariance between high-latitude and palaeoequatorial geochemical proxy records (Zhang et al., 1999; Royer, 2006; Montañez et al., 2007; Frank et al., 2008), confirming a relationship between pCO$_2$ and late Paleozoic climatic fluctuations on 10^6-yr.-order timescales.

Geochemical and other evidence from eastern Australia and beyond supports the interpretation that the P2 glacial interval was widespread, while glacial intervals P3 and P4 were more regionally limited (Fielding et al., 2008a, 2008b, 2008c; Frank et al., 2008; this study). Lines of evidence from this study include: 1) the larger magnitude of $\delta^{13}C_{org}$ shifts A and B (during P2) relative to those during P3 and P4, 2) concurrent shifts in $\delta^{13}C_{org}$ records from widely dispersed regions during P2, 3) a broad correlation between paleosol-derived pCO$_2$ values and the $\delta^{13}C_{org}$ and interpreted sedimentary record of climate from eastern Australia during P2 through P3. Geochemical proxy agreement during glacial intervals P3 and P4 is limited compared to that during P2. This may suggest that the interpreted pCO$_2$ and $\delta^{13}C_a$ changes during P3 and P4 in the eastern Australian record are somewhat smaller and not readily apparent in global proxy signals, which is in concordance with the model that glaciation across much of Gondwana had ceased but lingered in eastern Australia (Veevers & Powell, 1987; Isbell et al., 2003; Fielding et al., 2008c).

Cleal and Thomas (2005) note a marked correspondence between palaeotropical coal forest distribution and extent and late Paleozoic glaciation. Many studies have suggested enhanced terrestrial organic matter burial drove a drawdown of atmospheric CO$_2$ and the onset of high-latitude Carboniferous glaciation (e.g. Mii et al., 1999, 2001; Bruckschen et al., 1999; Saltzman, 2002), but Cleal and Thomas (2005) are among the first to recognize that the timing of early Permian expansion and mid-Permian contraction of Chinese and Far Eastern coal forests correlates with evidence of the overall timing of Permian glaciation from peak to waning icehouse conditions. Our interpretation that $\delta^{13}C_{org}$ shifts from the eastern Australian record reflect changes in atmospheric CO$_2$ driven by changes in organic matter burial in the terrestrial and/or marine realm supports the Permian model set out by Cleal and Thomas (2005) but is applied on shorter, several m.y.-order timescales to individual glacial intervals P2–P4.

Our interpretations suggest that variations in atmospheric CO$_2$ driven by changes in organic matter burial rates occurred on several m.y.-order timescales (~ 5–7 m.y., duration of P2, P3, and P4) during the Permian. An increasing number of studies, including this one, have found evidence of 10^6-yr.-order climatic variability on Gondwana during the late Paleozoic, specifically that glacial events alternated with periods of warmer climate (Amos & Lopez-Gamundi, 1981; Epshteyn, 1981a, 1981b; Sen, 1991; Chumakov, 1994; Osterloff et al., 2004; Raymond & Metz, 2004; Trosdtorf et al., 2005; Caputo et al., 2008; Fielding et

al., 2008c, Figure 2; Henry et al., 2008; Isbell et al., 2008a, 2008b; Martin et al., 2008; Mory et al., 2008; Stollhofen et al., 2008). Though glacial events appear somewhat asynchronous (Fielding et al., 2008c), such widespread similar patterns suggest 10^6-yr.-order climatic variability was typical of the polar late Paleozoic as a whole. Montañez et al. (2007) have constructed palaeoequatorial, geochemical, climate-proxy records that link these 10^6-yr.-order climatic changes recorded on Gondwana (Australia and Antarctica) to changes in pCO$_2$, (Montañez et al., 2007). Similar temporal patterns of glacial advance and deglaciation driven by global climatic-forcing factors are recognized from the geochemical and sedimentary record preserved in the Dwyka Group, Karoo Basin (Scheffler et al., 2003). Although the sedimentary products and models of deposition differ from those in eastern Australian succession, similar timescales (~ 5–7 m.y.) of climatic variability are documented (Visser, 1997; Bangert et al., 1999; Scheffler et al., 2003).

The magnitude of the timescale of climatic variability, 10^6-yr.-order, suggests a tectonic driver. Cleal and Thomas (2005) propose that temporal changes in organic matter burial rates, specifically peat formation, preservation, and extent, drove pCO$_2$ changes and glaciation. Peat formation, preservation and extent were ultimately controlled by various late Paleozoic mountain building events, which reduced peat formation, preservation, and extent in nearby regions during active tectonic periods. According to Cleal and Thomas (2005), China and the Far East account for the vast majority of Permian palaeotropical coal forests, but this region lacks known tectonic events that could modulate palaeotropical coal forest extent, and hence pCO$_2$ and glaciation, on several m.y.-order timescales. However, Permian Gondwanan coals are fairly common and can obtain significant thicknesses. Their potential significance and role in tectonically-driven changes in organic matter burial, pCO$_2$, and glacial extent have not been fully considered. Future work should be focused on identifying drivers of 10^6-yr.-order climatic variability during the late Paleozoic.

7. Conclusions

The composite $\delta^{13}C_{org}$ curve constructed using data from multiple formations exhibits excursions that reflect a combination of local and global scale controls. Changes in $\delta^{13}C_{org}$ due to local-scale controls, such as changes in organic matter source and other local environmental variables are apparent. However, global-scale controls associated with changes in rates of organic matter burial and preservation in terrestrial and/or marine environments are primary. Three positive (A, C, E) and three negative (B, D, F) $\delta^{13}C_{org}$ shifts occur at the beginning and mid- to end, respectively, of P2–P4 glacial intervals that have been documented across eastern Australia independently (Fielding et al., 2008a, 2008b). Proxy climate records from other regions of the globe display broadly synchronous variations, particularly during P2 glacial interval (Zhang et al., 1999; Royer, 2006; Montañez et al., 2007). We therefore interpret the broad features of the $\delta^{13}C_{org}$ curves associated with the P2–P4 glacial episodes to reflect global changes in atmospheric CO$_2$ (pCO$_2$ and/or the $\delta^{13}C_a$). Positive $\delta^{13}C_{org}$ shifts (A, C, E), which correlate with the onset of glacial intervals P2–P4, are interpreted to reflect increases in $\delta^{13}C_a$, and likely record periods of increased organic matter burial in terrestrial and/or marine settings, resulting in lower pCO$_2$ values. Conversely, negative $\delta^{13}C_{org}$ shifts (B, D, F), which correspond to the waning stages of glacials P2–P4, reflect decreases in $\delta^{13}C_a$, and, by inference, decreased rates of organic matter burial preservation and higher pCO$_2$ values.

Because $\delta^{13}C_{org}$ shifts can be linked directly to the high-latitude record of glaciation, the relationships between $\delta^{13}C_{org}$ and climatic shifts established herein may be used to guide future work. This study has succeeded in linking documented Permian climatic variability on several m.y.-order timescales to changes in pCO_2 and/or $\delta^{13}C_a$, based on an approach that combines geochemistry and sedimentary datasets. Other recent studies have found similar climatic variability on 10^6-yr.-order timescales during the late Paleozoic. Future work should focus on isolating pCO_2-related drivers of 10^6-yr. climatic variability during the late Paleozoic ice age.

Acknowledgments

References

Amos & Lopez-Gamundi, 1981 ◄ A. J. Amos and O. R. Lopez-Gamundi, Late Paleozoic Sauce Grande Formation in eastern Argentina. In: M. J. Hambrey and W. B. Harland, eds., *Earth's Pre-Pleistocene Glacial Record*, Cambridge University Press, Cambridge, U. K. (1981), pp. 872–877.

Arens et al., 2000 ◄ N. C. Arens, A. H. Jahren, and R. Amundson, Can C3 plants faithfully record the carbon isotopic composition of atmospheric carbon dioxide?, *Paleobiology* **26** (2000), pp. 137–164.

Bangert et al., 1999 ◄ B. Bangert, R. Armstrong, H. Stollhofen, and V. Lorenz, The geochronology and significance of ash-fall tuffs in the glaciogenic Carboniferous-Permian Dwyka Group of Nambia and South Africa, *Journal of African Earth Sciences* **29** (1999), pp. 33–49.

Bann et al., 2008 ◄ K. L. Bann, S. C. Tye, J. A. MacEachern, C. R. Fielding, and B. G. Jones, Ichnologic and sedimentologic signatures of mixed wave- and storm-dominated deltaic deposits: Examples from the Early Permian Sydney Basin, Australia. In: G. J. Hampson, R. Steel, P. Burgess, and R. Dalrymple, eds., *Recent Advances in Shallow-Marine Stratigraphy*, Society of Economic Paleontologists and Mineralogists (SEPM) Special Publication no. 90 (2008), pp. 293–332.

Birgenheier, 2007 ◄ Birgenheier, L. P., 2007. A sedimentologic, stratigraphic, and geochemical study of the late Paleozoic ice age, eastern Australia. Ph. D. Thesis, University of Nebraska-Lincoln, 263pp.

Birgenheier et al., 2009 ◄ L. P.Birgenheier, C. R. Fielding, M. C. Rygel, T. D. Frank, and J. Roberts, Evidence for dynamic climate change on sub-10^6-year scales from the late Paleozoic glacial record, Tamworth Belt, New South Wales, Australia, *Journal of Sedimentary Research* 79 (2009), pp. 56–82.

Bruckschen et al., 1999 ◄ P. Bruckschen, S. Oesmann, and J. Veizer, Isotope stratigraphy of the European Carboniferous; proxy signals for ocean chemistry, climate and tectonics, *Chemical Geology* **161** (1999), pp. 127–163.

Caputo et al., 2008 ◄ M. V. Caputo, J. H. Goncalves de Melo, M. Streel, and J. L. Isbell, Late Devonian and Early Carboniferous glacial records of South America. In: C. R. Fielding, T. D. Frank, and J. L. Isbell, eds., *Resolving the Late Paleozoic Ice Age in Time and Space*, Geological Society of America Special Publication vol. 441 (2008), pp. 161–174.

Chumakov, 1994 ◄ N. M. Chumakov, Evidence of late Permian glaciation in the Kolyma River Basin: A repercussion of the Gondwana glaciations in northeast Asia?, *Stratigraphy and Geological Correlation* **2** (5) (1994), pp. 426–444.

Cleal & Thomas, 2005 ◄ C. J. Cleal and B. A. Thomas, Paleozoic tropical rainforests and their effect on global climates: Is the past the key to the present?, *Geobiology* **3** (2005), pp. 13–31.

Domack et al., 1993 ◄ E. W. Domack, L. A. Burkley, C. R. Domack, and M. R. Banks, Facies analysis of glacial marine pebbly mudstones in the Tasmania Basin; implications for regional paleoclimates during the late Paleozoic. In: R. H. Findlay, R. Unrug, M. R. Banks, and J. J. Veevers, eds., *International Gondwana Symposium: Assembly, evolution and dispersal; proceedings of the Gondwana eight symposium. International Gondwana Symposium, International* (1993), pp. 471–484.

Epshteyn, 1981a ◄ O. G. Epshteyn, Late Permian ice-marine deposits of northeastern U. S. S. R. In: M. J. Hambrey and W. B. Harland, eds., *Earth's Pre-Pleistocene Glacial Record*, Cambridge University Press, Cambridge, U. K (1981), pp. 270–273.

Epshteyn, 1981b ◄ O. G. Epshteyn, Middle Carboniferous ice-marine deposits of northeastern U. S. S. R. In: M. J. Hambrey and W. B. Harland, eds., *Earth's Pre-Pleistocene Glacial Record*, Cambridge University Press, Cambridge U. K (1981), pp. 268–269.

Fielding et al., 2001 ◄ C. R. Fielding, R. Sliwa, R. J. Holcombe, and A. T. Jones, A new palaeogeographic synthesis for the Bowen, Gunnedah and Sydney basins of eastern Australia, *Petroleum Exploration Society of Australia Special Publication* **1** (2001), pp. 269–278.

Fielding et al., 2006 ◄ C. R. Fielding, K. L. Bann, J. A. MacEachern, S. C. Tye, and B. G. Jones, Cyclicity in the nearshore marine to coastal, Lower Permian, Pebbley Beach Formation, southern Sydney Basin, Australia; A record of relative sea-level fluctuations at the close of the late Palaeozoic Gondwanan ice age, *Sedimentology* **53** (2) (2006), pp. 453–463.

Fielding et al., 2008a ◄ C. R. Fielding, T. D. Frank, L. P. Birgenheier, M. C. Rygel, A. T. Jones, and J. Roberts, Stratigraphic imprint of the Late Paleozoic Ice Age in eastern Australia: A record of alternating glacial and nonglacial climate regime, *Geological Society of London Journal* **165** (2008), pp. 129–140.

Fielding et al., 2008b ◄ C. R. Fielding, T. D. Frank, L. P. Birgenheier, M. C. Rygel, A. T. Jones, and J. Roberts, Stratigraphic record and facies associations of the late Paleozoic ice age in eastern Australia (New South Wales and Queensland). In: C. R. Fielding, T. D. Frank, and J. L. Isbell, eds., *Resolving the Late Paleozoic Ice Age in Time and Space*, Geological Society of America Special Paper vol. 441 (2008), pp. 41–58.

Fielding et al., 2008c ◄ C. R. Fielding, T. D. Frank, and J. L. Isbell, The Late Paleozoic Ice Age — A review of current understanding and synthesis of global climate patterns. In: C. R. Fielding, T. D. Frank, and J. L. Isbell, eds., *Resolving the Late Paleozoic Ice Age in Time and Space*, Geological Society of America Special Publication vol. 441 (2008), pp. 343–354.

Frank et al., 2008 ◄ T. D. Frank, L. P. Birgenheier, I. P. Montanez, C. R. Fielding and M. C. Rygel, Controls on late Paleozoic climate revealed by comparison of near-field stratigraphic and far-field stable isotopic records. In: C. R. Fielding, T. D. Frank, and J. L. Isbell, eds., *Resolving the Late Paleozoic Ice Age in Time and Space*, Geological Society of America Special Paper vol. 441 (2008), pp. 331–342.

Gradstein et al., 2004 ◄ F. M. Gradstein, J. G. Ogg, and A. G. Smith, A Geologic Time Scale 2004, Cambridge University Press, Cambridge, U. K (2004).

Gröcke, 1998 ◄ D. R. Gröcke, Carbon-isotope analyses of fossil plants as a chemostratigraphic and palaeoenvironmental tool, *Lethaia* **31** (1998), pp. 1–13.

Gröcke, 2002 ◄ D. R. Gröcke, The carbon isotope composition of ancient CO_2 based on higher-plant organic matter, *Philosophical Transactions of the Royal Society of London, Mathematical, Physical and Engineering Sciences* **360** (2002), pp. 633–658.

Gröcke et al., 1999 ◄ D. R. Gröcke, S. P. Hesselbo, and H. C. Jenkyns, Carbon-isotope composition of Lower Cretaceous fossil wood; ocean-atmosphere chemistry and relation to sea-level change, *Geology* **27** (1999), pp. 155–158.

Gröcke et al., 2005 ◄ D. R. Gröcke, G. D. Price, S. A. Robinson, E. Y. Baraboshkin, J. Mutterlose, and A. H. Ruffell, The upper Valanginian (Early Cretaceous) positive carbon-isotope event recorded in terrestrial plants, *Earth and Planetary Science Letters* **240** (2005), pp. 495–509.

Grossman et al., 1993 ◄ E. L. Grossman, H. -S. Mii, and T. E. Yancey, Stable isotopes in Late Pennsylvanian brachiopods from the United States; implications for Carboniferous paleoceanography, *Geological Society of America Bulletin* **105** (1993), pp. 1284–1296.

Hayes et al., 1999 ◄ J. M. Hayes, H. Strauss, and A. J. Kaufman, The abundance of ^{13}C in marine organic matter and isotopic fractionation in the global biogeochemical cycle of carbon during the past 800 Ma, *Chemical Geology* **161** (1999), pp. 103–125.

Hedges & Stern, 1984 ◄ J. I. Hedges and J. H. Stern, Carbon and nitrogen determinations of carbonate-containing solids, *Limnology and Oceanography* **29** (1984), pp. 657–663.

Henry et al., 2008 ◄ L. C. Henry, J. L. Isbell, and C. O. Limarino, Carboniferous glacigenic deposits of the proto-Precordillera of west-central Argentina. In: C. R. Fielding, T. D. Frank, and J. L. Isbell, eds., *Resolving the Late Paleozoic Ice Age in Time and Space*, Geological Society of America Special Publication vol. 441 (2008), pp. 131–142.

Isbell et al., 2008a ◄ J. L. Isbell, D. I. Cole, and O. Catuneanu, Carboniferous–Permian glaciation in the main Karoo Basin, South Africa: Stratigraphy, depositional controls, and glacial dynamics. In: C. R. Fielding, T. D. Frank, and J. L. Isbell, eds., *Resolving the Late Paleozoic Ice Age in Time and Space*, *Geological Society of America Special Publication* vol. 441 (2008), pp. 71–82.

Isbell et al., 2008b ◄ J. L. Isbell, Z. J. Koch, G. M. Szablewski, and P. A. Lenaker, Permian glacigenic deposits in the Transantarctic Mountains, Antarctica. In: C. R. Fielding, T. D. Frank, and J. L. Isbell, eds., *Resolving the Late Paleozoic Ice Age in Time and Space*, *Geological Society of America Special Publication* vol. 441 (2008), pp. 59–70.

Isbell et al., 2003 ◄ J. L. Isbell, M. F. Miller, K. L. Wolfe, and P. A. Lenaker, Timing of late Paleozoic glaciation in Gondwana: Was glaciation responsible for the development of northern hemisphere cyclothems?. In: M. A. Chan and A. W. Archer, eds., *Extreme Depositional Dnvironments: Mega End Members in Geologic Time: Geological Society of America*, *Special Publication* **vol. 370** (2003), pp. 5–24.

Isozaki & Aljinovic, 2009 ◄ Y. Isozaki and D. Aljinovic, End-Guadalupian extincion of the Permian gigantic bivalve Ataloconchidae: End of gigantism in tropical seas by cooling. *Palaeogeography, Palaeoclimatology, Palaeoecology* 284 (2009), pp. 11–21.

Isozaki et al., 2007a ◄ Y. Isozaki, H. Kawahata, and K. Minoshima, The Capitanian (Permian) Kamura cooling event: The beginning of the Paleozoic–Mesozoic transition, *Palaeoworld* **16** (2007), pp. 16–30.

Isozaki et al., 2007b ◄ Y. Isozaki, H. Kawahata, and A. Ota, A unique carbon isotope record across the Guadalupian–Lopingian (Middle-Upper Permian) boundary in mid-oceanic paleo-atoll carbonates; The high-productivity "Kamura event" and its collapse in Panthalassa, *Global and Planetary Change* **55** (1–3) (2007), pp. 21–38.

James et al., 2009 ◄ N. P. James, T. D. Frank, and C. R. Fielding, Carbonate sedimentation in a Permian high-latitude, sub-polar depositional realm: Queensland, Australia, *Journal of Sedimentary Research* 79 (2009), pp. 123–143.

Keeling et al., 1979 ◄ C. D. Keeling, W. G. Mook, and P. P. Tans, Recent trends in the ^{13}C/ ^{12}C ratio of atmospheric carbon dioxide, *Nature* **277** (1979), pp. 121–123.

Korte et al., 2005 ◄ C. Korte, T. Jasper, H. W. Kozur, and J. Veizer, δ^{18}O and δ^{13}C of Permian brachiopods; A record of seawater evolution and continental glaciation, *Palaeogeography, Palaeoclimatology, Palaeoecology* **224** (2005), pp. 333–351.

Korte et al., 2008 ◄ C. Korte, P. J. Jones, U. Brand, D. Mertmann, and J. Veizer, Oxygen isotope values from high-latitudes: Clues for Permian sea-surface temperature gradients and Late Paleozoic deglaciation, *Palaeogeography, Palaeoclimatology, Palaeoecology* **269** (2008), pp. 1–16.

Marino & McElroy, 1991 ◄ B. D. Marino and M. B. McElroy, Isotopic composition of atmospheric CO$_2$ inferred from carbon in C4 plant cellulose, *Nature* **349** (1991), pp. 127–131.

Martin et al., 2008 ◄ J. R. Martin, J. Redfern, and J. F. Aitken, A regional overview of the late Paleozoic glaciation in Oman. In: C. R. Fielding, T. D. Frank, and J. L. Isbell, eds., *Resolving the Late Paleozoic Ice Age in Time and Space*, *Geological Society of America Special Publication* vol. 441 (2008), pp. 175–186.

Meyers, 1997 ◄ P. A. Meyers, Organic geochemical proxies of paleoceanographic, paleolimnologic, and paleoclimatic processes, *Organic Geochemistry* 27 (1997), pp. 213–250.

Meyers et al., 1995 ◄ P. A. Meyers, M. J. Leenheer, and R. A. Bourbonniere, Diagenesis of vascular plant organic matter components during burial in lake sediments, *Aquatic Geochemistry* **1** (1995), pp. 35–52.

Mii et al., 1999 ◄ H. -S. Mii, E. L. Grossman, and T. E. Yancey, Carboniferous isotope stratigraphies of North America; Implications for Carboniferous paleoceanography and Mississippian glaciation, *Geological Society of America Bulletin* 111 (1999), pp. 960–973.

Mii et al., 2001 ◄ H. -S. Mii, E. L. Grossman, T. E. Yancey, B. Chuvashov, and A. Egorov, Isotopic records of brachiopod shells from the Russian Platform; evidence for the onset of Mid-Carboniferous glaciation, *Chemical Geology* 175 (2001), pp. 133–147.

Montañez et al., 2007 ◄ I. P. Montañez, N. J. Tabor, D. Niemeier, W. A. DiMichele, T. D. Frank, C. R. Fielding, J. L. Isbell, L. P. Birgenheier, and M. C. Rygel, CO$_2$-forced climate instablility and linkages to tropical vegetation during late Paleozoic deglaciation, *Science* 315 (2007), pp. 87–91.

Mory et al., 2008 ◄ A. J. Mory, J. Redfern and J. R. Martin, A review of Permian–Carboniferous glacial deposits in Western Australia. In: C. R. Fielding, T. D. Frank, and J. L. Isbell, eds., *Resolving the Late Paleozoic Ice Age in Time and Space*, *Geological Society of America Special Publication* **vol. 441** (2008), pp. 29–40.

Osterloff et al., 2004 ◄ P. Osterloff, R. Penney, J. Aitken, N. Clark, and M. I. Al-Husseini, Depositional sequences of the Al Khlata Formation, subsurface interior Oman, *GeoArabia Manama* **9** (2004), p. 155.

Pagani, 2002 ◄ M. Pagani, The alkenone-CO$_2$ proxy and ancient atmospheric carbon dioxide, *Philosophical Transactions - Royal Society of London*, Royal Society of London, London, United Kingdom, United Kingdom (2002), pp. 609–632.

Raymond & Metz, 2004 ◄ A. L. Raymond and C. Metz, Ice and its consequences; glaciation in the Late Ordovician, Late Devonian, Pennsylvanian–Permian, and Cenozoic compared, *Journal of Geology* **112** (6) (2004), pp. 655–670.

Rimmer et al., 2006 ◄ S. M. Rimmer, H. D. Rowe, D. N. Taulbee, and J. C. Hower, Influence of maceral content on δ^{13}C and δ^{15}N in a Middle Pennsylvanian coal, *Chemical Geology* **225** (2006), pp. 77–90.

Rogala et al., 2007 ◄ B. Rogala, N. P. James, and C. M. Reid, Deposition of Polar carbonates during interglacial highstands on an Early Permian shelf, Tasmania, *Journal of Sedimentary Research* 77 (2007), pp. 587–606.

Royer, 2006 ◄ D. L. Royer, CO$_2$-forced climate thresholds during the Phanerozoic, *Geochimica et Cosmochimica Acta* 70 (2006), pp. 5665–5675.

Royer et al., 2004 ◄ D. L. Royer, R. A. Berner, I. P. Montanez, N. J. Tabor, and D. J. Beerling, CO$_2$ as a primary driver of Phanerozoic climate, *Geological Society of America Today* 14 (3) (2004), pp. 4–10.

Rygel et al., 2008 ◄ M. C. Rygel, C. R. Fielding, K. L. Bann, T. D. Frank, L. Birgenheier, and S. C. Tye, The early Permian Wasp Head Formation, Sydney Basin: High-latitude shallow marine sedimentation following the late Asselian–Early Sakmarian glacial event in eastern Australia, *Sedimentology* **55** (2008), pp. 1517–1540.

Saltzman, 2002 ◄ M. R. Saltzman, Carbon and oxygen isotope stratigraphy of the Lower Mississippian (Kinderhookian–Lower Osagean), Western United States; Implications for seawater chemistry and glaciation, *Geological Society of America Bulletin* 114 (2002), pp. 96–108.

Saltzman, 2003 ◄ M. R. Saltzman, Late Paleozoic ice age; oceanic gateway or pCO$_2$?, *Geology Boulder* 31 (2003), pp. 151–154.

Scheffler et al., 2003 ◄ K. Scheffler, S. Hoernes, and L. Schwark, Global changes during Carboniferous–Permian glaciation of Gondwana:Linking polar and equatorial climate evolution by geochemical proxies, *Geology* 31 (2003), pp. 605–608.

Sen, 1991 ◄ D. P. Sen, Sedimentation patterns of the Talchir Group in the Giridih Gondwana Basin, India: A case of multiple glacial advance and retreat, *Palaeogeography, Palaeoclimatology, Palaeoecology* **86** (1991), pp. 339–352.

Shearman & Smith, 1985 ◄ D. J. Shearman and A. J. Smith, Ikaite, the parent mineral of jarrowite-type pseudomorphs, *Proceedings of the Geologists' Association* **96** (4) (1985), pp. 305–314.

Stollhofen et al., 2008 ◄ H. Stollhofen, M. Werver, I. G. Stanistreet, and R. A. Armstron, Single-zircon U–Pb dating of Carboniferous–Permian tuffs, Namibia, and the intercontinental deglaciation cycle framework. In: C. R. Fielding, T. D. Frank, and J. L. Isbell, eds., *Resolving the Late Paleozoic Ice Age in Time and Space*, *Space, Geological Society of America Special Publication* vol. 441 (2008), pp. 83–96.

Trosdtorf et al., 2005 ◄ I. Trosdtorf Jr., A. C. Rocha-Campos, P. R. dos Santos, and A. Tomio, Origin of late Paleozoic, multiple, glacially striated surfaces in northern Parana Basin (Brazil): Some implications for the dynamics of the Parana glacial lobe, *Sedimentary Geology* **181** (2005), pp. 59–71.

Veevers & Powell, 1987 ◄ J. J. Veevers and M. Powell, Late Paleozoic glacial episodes in Gondwanaland reflected in transgressive–regressive depositional sequences in Euramerica, *Geological Society of America, Bulletin* **98** (1987), pp. 475–487.

Veizer et al., 1999 ◄ J. Veizer, D. Ala, K. Azmy, P. Bruckschen, D. Buhl, F. Bruhn, G. A. F. Carden, A. Diener, S. Ebneth, Y. Godderis, T. Jasper, C. Korte, F. Pawellek, O. G. Podlaha, and H. Strauss, ^{87}Sr/^{86}Sr, δ^{13}C and δ^{18}O evolution of Phanerozoic seawater, *Chemical Geology* **161** (1999), pp. 59–88.

Visser, 1997 ◄ J. N. J. Visser, Deglaciation sequences in the Permo-Carboniferous Karoo and Kalahari basins of Southern Africa: A tool in the analysis of cyclic glaciomarine basin fills, *Sedimentology* **44** (1997), pp. 507–521.

Zhang et al., 1999 ◄ H. Zhang, G. Shen, and Z. He, A carbon isotopic stratigraphic pattern of the late Palaeozoic coals in the North China Platform and its palaeoclimatic implications, *Acta Geologica Sinica English Edition* **73** (1999), pp. 111–119.